INTERNATIONAL JOURNAL OF HYDROGEN ENERGY 47 (2022) 27303–27325

Available online at www.sciencedirect.com

ScienceDirect

journal homepage: www.elsevier.com/locate/he

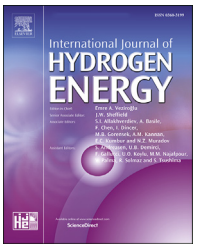

Assessing sizing optimality of OFF-GRID AC-linked solar PV-PEM systems for hydrogen production

Felipe Gallardo [a,*], *José García* [a], *Andrea Monforti Ferrario* [b,c], *Gabriele Comodi* [b], *Justin NW. Chiu* [a]

[a] *Royal Institute of Technology, KTH, Department of Energy Technology, Brinellvägen 68, Stockholm SE-100 44, Sweden*

[b] *Department of Industrial Engineering and Mathematical Sciences, Marche Polytechnic University, Ancona, Italy*

[c] *ENEA, Italian National Agency for New Technologies, Energy and Sustainable Economic Development, Department of Energy Technologies and Renewable Sources, Laboratory of Energy Storage, Batteries and Hydrogen Production & Use (TERIN-PSU-ABI). Via Anguillarese, 00123 Rome, Italy*

HIGHLIGHTS

- The AC/AC ratio (PV-inverter to PEM capacity) is proposed as optimization variable.
- Low solar resource leads to large solar plant oversizing and high AC/AC ratios.
- In Atacama, Chile, an AC/AC = 1.2 & DC/AC = 1.3 leads to an optimal LCOH = 5.9 USD/kg.
- In Fargo, N. Dakota, an AC/AC = 1.4 & DC/AC = 1.8 leads to an optimal LCOH = 9.7 USD/kg.
- The optimal PV plant DC/AC can vary up to 54% if minimizing energy or hydrogen cost.

ARTICLE INFO

Article history:
Received 8 April 2022
Received in revised form
26 May 2022
Accepted 10 June 2022
Available online 7 July 2022

Keywords:
Solar hydrogen
Techno-economic analysis

ABSTRACT

Herein, a novel methodology to perform optimal sizing of AC-linked solar PV-PEM systems is proposed. The novelty of this work is the proposition of the solar plant to electrolyzer capacity ratio (AC/AC ratio) as optimization variable. The impact of this AC/AC ratio on the Levelized Cost of Hydrogen (LCOH) and the deviation of the solar DC/AC ratio when optimized specifically for hydrogen production are quantified. Case studies covering a Global Horizontal Irradiation (GHI) range of 1400–2600 kWh/m^2-year are assessed. The obtained LCOHs range between 5.9 and 11.3 USD/kgH_2 depending on sizing and location. The AC/AC ratio is found to strongly affect cost, production and LCOH optimality while the optimal solar DC/AC ratio varies up to 54% when optimized to minimize the cost of hydrogen instead of the cost of energy only. Larger oversizing is required for low GHI locations; however, H_2 production is more sensitive to sizing ratios for high GHI locations.

* *Corresponding author.*
E-mail address: figallar@kth.se (F. Gallardo).

https://doi.org/10.1016/j.ijhydene.2022.06.098

Nomenclature

AC/AC	AC Power ratio: electrolyzer to solar inverter
ALK	Alkaline electrolyzer
BoP	Balance of Plant
CAPEX	Capital Expenditures
DC/AC	Power ratio: Solar PV to Solar inverter
GHG	Greenhouse Gases
GHI	Global Horizontal Irradiation
GWP	Global Warming Potential
HHV	Higher Heating Value
LCOE	Levelized Cost of Electricity
LCOH	Levelized Cost of Hydrogen
NPV	Net Present Value
OP	Voltage Over-potentials
OPEX	Operational Expenditures
p.u.	Per Unit
PEM	Proton Exchange Membrane
PV	Photovoltaics
PV-EL:	Photovoltaic-fed electrolysis
SOEC	Solid Oxide Electrolyzer
TOTEX	Total Expenditures
WACC	Weighted average cost of capital

Symbols and notations

A_{cell}^{active}	Active cell area (cm^2)
AC/AC	AC/AC ratio (–)
E_{cell}	Cell voltage (V)
E_{cell}^{OC}	Open circuit cell voltage (V)
E_{th}	Thermoneutral voltage (V)
ε_F	Faraday efficiency (%)
ε_v	Voltage efficiency (%)
Energy output	Energy output (MWh/year)
F	Faraday constant (C/mole-)
ΔH_R	Enthalpy of reaction (kJ/mol)
$H_{2_{(t)}}$	Hydrogen production (kg/year)
j	Current density (A/cm2)
$LCOH$	Levelized Cost of Hydrogen (USD/kg)
$m_{H_2}^{ideal}$	Hydrogen flow rate (ideal) (mol/s)
$\dot{m}_{H_2}^{real}$	Hydrogen flow rate (real) (mol/s)
n	Stoichiometric factor (mole-/molH2)
$N_{\frac{cells}{stack}}$	Number of cells per stack (#)
$NPV_{cos\ ts}$	Net Present Value (USD)
$OPEX_{(t)}$	Operating Expenditures (USD/year)
P_{PEM}^{AC}	PEM Electrolyser nominal power (AC) (kW)
P_{an}	Pressure anode compartment (bar)
P_{inv}^{AC}	Inverter nominal power (kW)
P_{stack}^{in}	Electrolyser input power (kW)
t	Years (year)
T_{op}	Operating temperature (°C)
V_{act}	Activation overpotential (V)
V_{diff}	Diffusion overpotential (V)
V_{ohm}	Ohmic overpotential (V)

Introduction

Context

Hydrogen (H_2), when produced in processes with low Global Warming Potential (GWP) burdens, is broadly acknowledged as a valuable energy vector capable of enabling the decarbonization of challenging sectors such as the chemical industry, steel manufacturing or heavy-duty transportation [1–3]. When produced from electrolysis of water powered by renewable energy sources, oxygen is the main by-product of the process and there are no direct emissions of Greenhouse Gases (GHG) during the operation phase; thus the produced H_2 is said to be "green" [4]. In addition, green hydrogen-based storage systems are recognized as one of the most relevant pathways to integrate large quantities of intermittent renewable energy sources, provide seasonal storage services and bridge the gap in otherwise hard-to-couple energy systems such as heating, transport and electricity [5]. Furthermore, the adoption of green H_2 has been pointed out as a feasible climate change mitigation pathway by the Intergovernmental Panel on Climate Change (IPCC) [6–8].

Green H_2 presents the least GWP burdens compared to other H_2 production pathways, but it is currently more expensive to produce than the most common H_2 production pathways based on fossil fuels, also known as fossil H_2 or blue H_2 when carbon capture is implemented [3,4,9]. Fossil H_2 production pathways are low in cost but heavily intensive in GWP burdens.

Moreover, despite the current international enthusiasm for green H_2, of the total 90 Mt of H_2 consumed in the world in 2020, around 80% came from fossil fuels pathways, mostly from unabated processes, and the rest mainly from residual gases from the petrochemical industry, causing total emissions for around 900 Mt of CO_2 equivalent [10]. Thus, the importance and urgency to develop and optimize green H_2 production pathways.

One pathway to produce green H_2 is the use of solar photovoltaic (PV) power plants supplying power to electrolysis systems, therefore ensuring a zero-emission energy supply. This is known as photovoltaic-electrolytic water splitting (PV-EL) which is the focus of this study. As discussed later in section 2, there are several topological possibilities to connect solar PV to PEM electrolyzers. In this study we focus on off-grid solar systems coupled via an AC-link to PEM electrolyzers as shown in Fig. 1, where the electricity from the PV panels is transformed from DC to AC using inverters, and then used by the electrolyzers via AC/DC rectifiers. Herein, this type of system will be referred to as off-grid AC-linked PV-PEM.

Despite the relevance of the demand and use phase for project specific analysis, in this work we focus on the production phase only and in the elements driving its optimal sizing and design.

Scope of work

The scope of this work is to study the optimal size of off-grid AC linked PV-PEM systems and to assess the relative sizing ratios between components (solar PV, inverter, electrolyser) with a fully integrated approach under different solar resource conditions. The effect of this relative sizing ratios is considered with a model-based approach in terms of the techno-economic performance of the solar-hydrogen plant.

Original contribution and motivation of relevant work

Although solar-hydrogen systems represent a well-known topic in scientific literature, a fully integrated optimization of the relative sizing of all the components is typically not assessed (either the solar section or the hydrogen section is optimized separately). In particular the AC/AC ratio has not been studied until now as separate optimization variable to the best knowledge of the authors, which is the main original contribution of this work. The integrated optimization approach allows to investigate trends and patterns of the integrated plant optimality with both the aforementioned relative sizing ratios, achieving different results with respect to non-integrated optimization approaches.

Despite a simple system configuration, the integrated optimization analysis with the additional AC/AC ratio parameter is relevant since AC-linked systems represent the most commercially mature plant configuration which is expected to compose most of the future PV-EL installed capacity. Thus, integrated PV-EL system optimization represents an urgent knowledge gap which this work aims to fill to provide indications on optimal PV-EL plant configurations and their impact on hydrogen cost, which can be readily transferred to market.

Background

Green hydrogen and the use of off grid PV-PEM systems to produce it, have gained interest due to several technical, environmental, economic and political factors. These factors include the increasing price of conventional fuel, the urgent need to reduce dependence on fossil generation due to environmental reasons, the geopolitical dependence of European countries on external supplies of oil and gas, and the progress made in electrolysis efficiency in the last decades. This political and techno-economic scenario is the context of the recent international interest in solar pathways to produce hydrogen at competitive prices [9,11–14]. Available literature covers modelling, design and optimization of PV-EL systems extensively.

Most studies focus on directly coupled systems via direct DC links between the solar array and the electrolyzer [15–26]. These present low costs and, provided that the matching design between PV-array-output and electrolyzer-input is optimal, which is not trivial [21], these systems can reach high maximum efficiency [15–17,20]. However, they can only reach optimal efficiency during the hours where the solar input and meteorological conditions meet the design point, which can be highly challenging depending on the site [18]. Moreover as these systems lack Maximum Power Point Tracker systems (MPPT) in their topology, PV array voltage and current outputs cannot be controlled to deliver maximum power at any given solar condition, thus compromising the average efficiency of the hybrid system during the year [23–26].

Another option that has been studied extensively is the use of PV-EL coupled via DC/DC converters. These systems present more integration and components, therefore higher CAPEX and lower maximum efficiency than directly coupled but they can reach higher average efficiency due to the use of MPPT [25–30].

The comparative amount of research found on AC-coupled PV-EL systems (DC/AC-AC/DC) [31–33] is considerably less. Additionally, most research regarding system analysis and optimization focuses on dispatch optimization rather than optimal sizing at sub-system level. In fact, most studies found about PV-EL optimization in the early 2010s, focused on finding optimal operational setups and dispatching strategies for systems with either direct DC links between the solar plant and the electrolyzer or systems connected via DC/DC links [15–18,28,29,34], including electrolyzers PEM, Alkaline (ALK) and Solid Oxide (SOEC). Furthermore, as mentioned by Gibson et al. in Ref. [15], AC-linked PV-EL systems were considered less competitive than DC-linked systems due to the extra cost of the inverter equipment and the loss in efficiency.

However, as it also happens with other DC technologies such as battery energy systems, there are no standard topologies valid for all setups and the actual designs are strongly project-dependent [35,36]. In this context, and due to the drastic cost reductions, efficiency improvements and commercial maturity reached by inverter technologies and AC systems in general, AC-links can be a feasible pathway to couple solar PV systems to any type of downstream assets [26]. In power systems, these assets can include DC devices with integrated AC/DC rectifiers as it is normally the case of batteries and more importantly for the scope of this study, electrolyzers [37]. A summary of the literature consulted regarding solar PV-EL system analysis for this background section is presented in Table 1.

Thus, the topological pathway assessed in this study, off-grid PV-PEM AC-linked systems, is of interest given the drastic progress in technological and economic aspects, such as efficiency improvements and sharp investment cost reductions of both solar PV [38,39] and electrolysis systems [40] in the last two decades. In particular, PEM technology has evolved from a cost per stack as high as 4700 €/kW in the 90s to current costs near 1000 €/kW, while forecasted costs of 500 €/kW are expected to be reached by 2030 for utility scale projects or MW-scale stacks [11,40–42].

Currently, PEM electrolyzers are considered to be among the most apt for off grid system designs and PV-coupling due to its operational flexibility and suitability to withstand fast dynamic changes in power supply [43]. Additionally, PEM electrolyzers allow for higher hydrogen outlet pressure, lower gas crossover and higher H_2 purity, higher cell current densities, wider and faster operational range, higher voltage efficiency, more compact designs and are lighter in mass compared to ALK electrolyzers [44–46]. Notwithstanding that PEM electrolyzers are currently more expensive than ALK, PEM costs are expected to further decrease while increasing

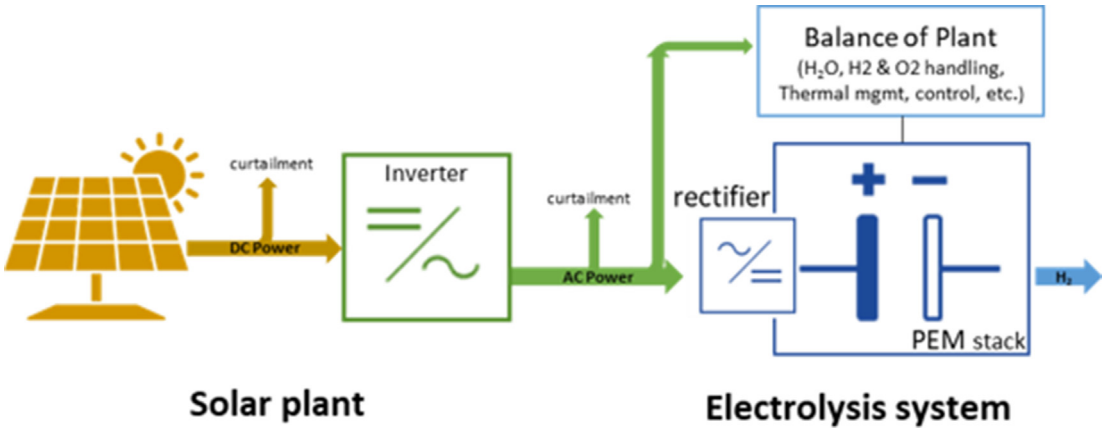

Fig. 1 – Solar hydrogen off-grid standalone production scheme.

overall efficiency in the coming decades due to the maturity of large scale-up projects being developed worldwide [41,42]. A third well-known type of electrolyzer is based on solid oxide electrolysis cells (SOEC). This technology is more efficient in terms of energy consumption; however, it relies on thermal integration to other processes and is not as mature and commercially ready as PEM and ALK. Table 2 summarizes the most important technical and economic characteristics of these electrolyzer technologies.

Methodology

General methodology

This study was developed based on performance simulations for off-grid stand-alone H_2 plants constituted by solar PV and PEM-electrolysis systems. The system was modelled at subsystem level to provide results with hourly resolution in a multi-year horizon for user-defined locations.

The PEM electrolysis system model was developed as an in-house model coded in Python at component-level including efficiency curves for both stack and Balance of Plant (BoP) validated with results from literature review. For the solar PV system and inverter models; the open source library PySAM was used. For the system's optimal sizing, an in-house project performance simulator able to cover a user-defined spectrum of design capacities of solar PV, solar inverters and PEM capacity was implemented.

Simulations for each configuration were performed with output results on hourly H_2 production, power curtailment, water consumption and degradation, as well as Capital Expenditures (CAPEX), Operational Expenditures (OPEX), project Net Present Value (NPV), solar LCOE and final LCOH. This can be done for each configuration within a user-defined spectrum in location-dependent multi-year scenarios thus allowing finding the optimal design for each scenario. The operational results of each assessed design combination are post-processed and compared by examining metrics such as LCOH, electrolyzer utilization factor and roundtrip energy efficiency. A flowchart of this methodology is shown in Fig. 2.

Case studies

A project location defines the solar resource availability and meteorological conditions that would affect the performance of a project. Thus, the proposed methodology is applied within a set of three different locations for which the Typical Meteorological Years (TMY) for environmental data and GHI are considered as shown in Table 3.

Configurations

For each project location, a spectrum of feasible project configurations is defined keeping the solar PV capacity set at 27 MW. The DC/AC ratio ranges between one and two, which allows obtaining an envelope for the sizing spectrum covering from a system with no DC/AC oversizing to a one with a solar field oversized two times compared to the inverter. To cover this DC/AC range, the inverter AC capacity is varied from 27 MW to 13.9 MW while keeping the solar PV capacity fixed as shown in Table 4.

For the total electrolysis input capacity, a spectrum of AC capacities is studied. The AC/AC ratio is defined in Equation (1), below where P_{inv}^{AC} is the total AC capacity of the solar inverters (MW) and , P_{PEM}^{AC} is the total electrolysis nominal AC input capacity (MW).

$$AC \Big/ AC\ ratio: \frac{P_{inv}^{AC}}{P_{PEM}^{AC}} \tag{1}$$

For each DC/AC configuration defined, the AC/AC ratio is varied from one to two by considering different electrolysis capacities coupled downstream of the solar inverter. Therefore, to vary the AC/AC ratio, the installed electrolysis capacity is varied as shown in Table 5.

Solar system costs and projections

Based on [26,50,51], the solar PV cost was set at 400 USD/kW_{dc} for the PV modules, 100 USD/kW_{dc} for solar BOP (equipment and installation not including the inverter) and 100 USD/kW_{dc} for development costs (Permitting, Environmental studies, EPC, land and margins) with a total overnight cost of 600 USD/

Table 1 – Review on similar PV-EL studies, organized by EL technology and PV-EL link type.

Author	Ref.	EL	PV-EL link	Focus
Gibson and Kelly	[15]	PEM	Direct link	Design, operation
Yang et al.	[16]	ALK	Direct link	Modelling, operation
Khalilnejad et al.	[17]	ALK	Direct link	Design, operation
Sayedin et al.	[18]	PEM	Direct link	Optimal sizing
Navarro-Solís et al.	[19]	PEM	Direct link	Experimental, component design
Ferrero and Santarelli	[20]	PEM	Direct link	Experimental, modelling
Paul and Andrews	[21]	PEM	Direct link	Experimental, design, operation
Shapiro et al.	[22]	PEM	Direct link	Experimental, operation
Cai et al.	[23]	PEM	Direct link	Experimental, operation
Atlam et al.	[24]	PEM	Direct link	Design, operation
Grube et al.	[25]	PEM SOE	DC/DC converter and direct link	Design, economic.
M. Reuβ et al.	[26]	PEM	3 direct link and 1 DC/DC converter	Design, operation, economic
Ceylan and Devrim	[27]	PEM	DC/DC converter	Design, operation, modelling
Ghribi et al.	[28]	PEM	DC/DC converter	Experimental, modelling
Scamann et al.	[29]	PEM	DC/DC converter	Component design
Aouali et al.	[30]	PEM	DC/DC converter	Experimental, modelling
Khelfaoui et al.	[31]	PEM	DC/AC-AC/DC	Experimental, modelling, operation
Papadopoulos et al.	[32]	PEM	DC/AC-AC/DC	Design, operation
Tang et al.	[33]	PEM	DC/AC-AC/DC	Economic modelling

kW_{dc} installed for the solar plant without inverter. The grid-forming inverter was assumed to have a cost of 70 USD/kW_{ac}. The O&M annual cost of the solar plant was set at 40 USD/kW_{dc}.

Electrolysis costs

The costs of the PEM system including stack and modular BoP are based on multiple references [11,40,42]. They would amount to 1200 USD/kW_{ac} and the development cost for the plant 500 USD/kW_{ac} with a total overnight CAPEX of 1700 USD/kW_{ac} for the installed electrolysis system. The annual O&M cost was estimated to be 2% of the electrolyzer CAPEX. The cost of tap water considered was 2 USD/m^3.

Financial assumptions

Since these type of projects are intensive in CAPEX, a rather simplified project finance structure was considered to enable the assessment of the classic economic performance metrics. In particular, a Weighted Average Cost of Capital (WACC) of 7% and a project financial horizon of 20 years. Therefore, in this study for all the metrics that imply a certain value of money in time such as NPV, LCOE or LCOH (formulas stated in section IV), the latter parameters for WACC and financial horizon were used. In Table 6, a summary of the economic parameters, costs and financial assumptions used in this study is presented.

Table 3 – Location and solar resource of the case studies.

Location	GHI [kWh/m^2-year]	Source TMY
M[a] Elena, Atacama, CL	2′639	Energy Ministry CL [48].
Phoenix, AZ, USA	2′113	NSRDB [49]
Fargo, ND, USA	1′405	NSRDB [49]

System modelling

Solar PV plant and inverter models

The solar PV system was modelled using the module "Detailed Photovoltaic Model" available in PySAM [51] which is a publicly available wrapper for the modules of the software System Advisor Model (SAM), developed by NREL [52]. The used detailed PV model estimates the power output of the PV plant based on an implementation developed by SAM of a semi-empirical, 5-parameter, one-diode equivalent

Table 2 – Techno-economic characteristics of electrolyzers [11,44,47].

	ALK		PEM		SOEC	
	Now	Long term	Now	Long term	Now	Long term
Electrical eff. (LHV) [%]	63–70		56–60	67–74	74–81	77–90
Operating pressure [bar]	1–30		30–80		1	
Operating T. [°C]	60–80		50–80		650–1000	
Stack lifetime [1000 op. hours]	60–900	100–150	30–90	100–150	10–30	75–100
Load range (of nominal) [%]	10–110		0–160		20–100	
Plant footprint [m^2/kW_e]	0.095		0.048			
CAPEX [kUSD/kW_e]	0.5–1.4	0.2–0.7	1.1–1.8	0.2–0.9	2.8–5.6	0.5–1

circuit performance model following the California Energy Commission guidelines [53,54] and an inverter model. This module, accounts for the effect of temperature on module performance, and has options for calculating shading and other losses in the system [53].

The parametrical values defining the system's components such as type of PV module used and inverter were taken from the publicly available catalogue of the software. In particular, the PV system model is ground-mounted with single axis tracking constituted by 310 W mono-c-Si PV modules SunPower SPR-E19-310-COM with a nominal efficiency of 19% and an annual DC degradation of 0.5%. The solar PV DC capacity was arbitrarily set at 27 MW to represent a large-scale project. The system was optimally modelled according to latitude with a Ground Covering Ratio of 0.3. Total DC losses amount 4.4% including wiring, module mismatch and connections. The AC losses were considered 1% due to wiring. The shading effect was not considered and the soiling was assumed to account for 5% of annual losses. 770kW$_{ac}$ Inverters SMA America SC750CP-US with a nominal efficiency of 97.37% were considered. Ten values for the solar DC/AC ratio were considered and parametrized to vary between [1,2] in steps of 0.1 adjusting for that purpose the inverter AC capacity while keeping fixed the PV DC capacity. These are arbitrary design choices made considering the available components in SAM's libraries.

Table 4 – DC/AC ratio optimization spectrum.

Inverters count	Inverter capacity [MWac]	DC/AC ratio
35	27.0	1.0
33	25.6	1.1
32	24.3	1.1
30	22.9	1.2
28	21.6	1.3
26	20.2	1.3
25	18.9	1.4
23	17.5	1.5
21	16.2	1.7
19	14.8	1.8
18	13.5	2.0

Electrolysis system

The electrolysis system was modelled to be formed by containerized modules of 220 kW PEM stacks with their

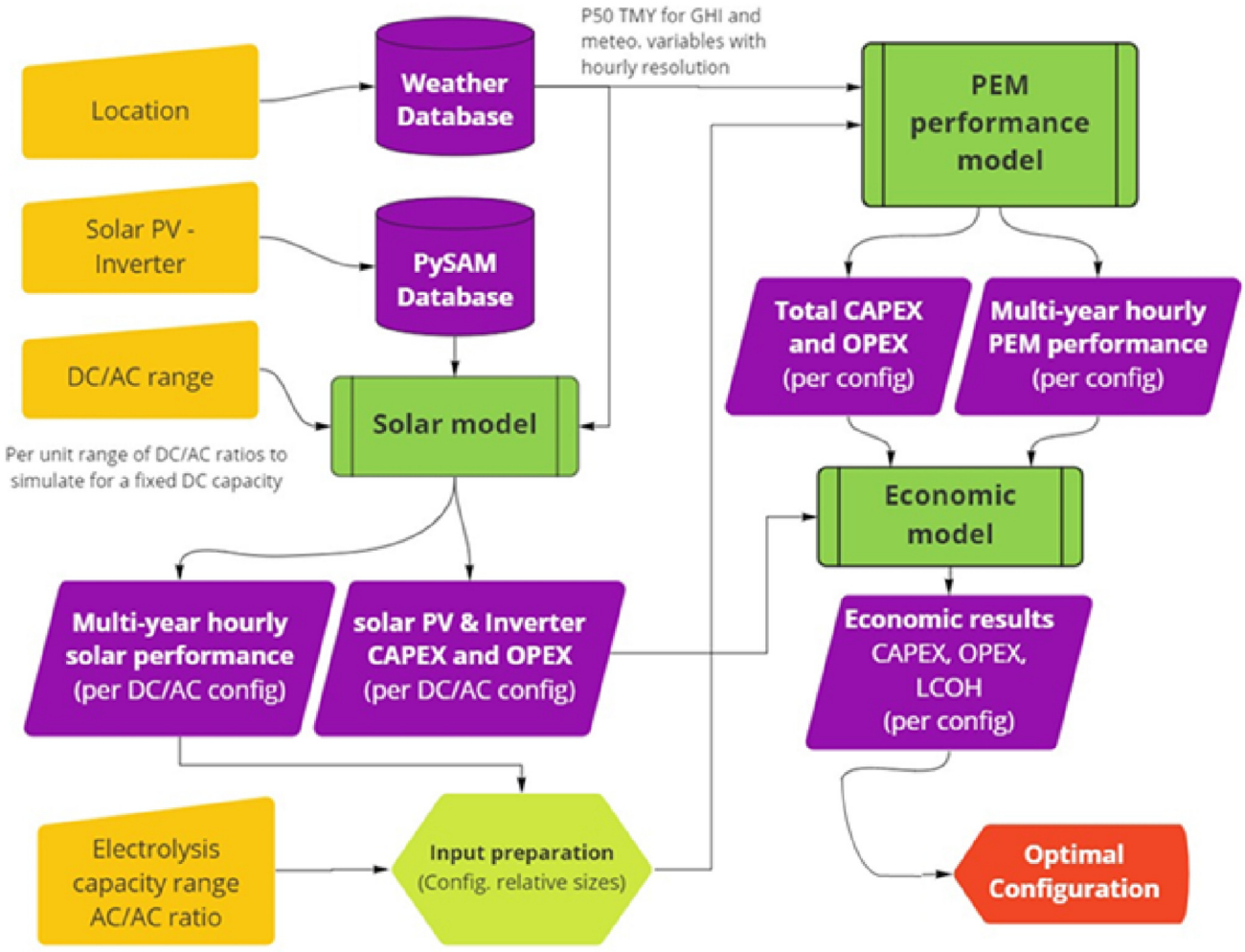

Fig. 2 – Methodology flow chart.

respective modules of 40 kW BoP according to Ref. [55]. For this purpose, a 3-variable steady-state parametric model at component level was designed following the guidelines proposed by Falcao et al. in Ref. [56] for parametric modelling of PEM stacks and the generic parameters of a 220 kW PEM stack and BOP system reported by NREL in Ref. [55]. The three variables defining the operation of the electrolyzer cell and therefore of the stack, are operating temperature, pressure and current density.

PEM cell model

The steady-state model of the PEM cell is obtained by modelling the voltage behaviour of the cell or polarization curve. In this model, the polarization curve of the cell is obtained with four equations and is dependent on operational temperature, partial pressures, and current density [57]. The main parameters defining the cell were taken from Ref. [55] and are shown in Table 7.

The behaviour of the PEM cell voltage is then simulated by modelling the voltage efficiency ε_V (Equation (2)) and the Faraday efficiency ε_F (Equation (3)). The voltage efficiency ε_V is defined as the ratio between the thermo-neutral E_{th} potential (which is defined as the minimum electrical work needed to split water in isothermal conditions) and the actual cell voltage E_{cell} under operation [58], valid as long as $E_{cell} > E_{th}$ while the Faraday efficiency ε_F is defined as the ratio between $\dot{m}_{H2}^{real}$ the actual H_2 mass flow outlet under operation and $\dot{m}_{H2}^{ideal}$ its theoretical maximum, at the specific operating current [59]. The total efficiency of the cell ε_{cell} (Equation (4)) is the product of voltage efficiency and faraday efficiency. The latter is assumed to be a fixed value set at 96%, which is a typical value for medium-high current density operating points [60].

$$\varepsilon_V = \frac{E_{th}}{E_{cell}} \tag{2}$$

$$\varepsilon_F = \frac{\dot{m}_{H_2}^{real}}{\dot{m}_{H_2}^{ideal}} \tag{3}$$

$$\varepsilon_{cell} = \varepsilon_V \cdot \varepsilon_F \tag{4}$$

At standard thermodynamic conditions E_{th}^0 is calculated as the ratio between the reaction enthalpy of water in standard conditions ΔH_R^0 equal to −285.83 kJ/mol and the product between the faraday constant F (96,485C/mol_{e^-}) and the number moles of electrons transferred per mole of hydrogen during the reaction and $n = 2$ mol_{e^-}/mol_{H2} (Equation (5)) [56,58,59].

$$E_{th}^0 = \frac{\Delta H_R^0}{nF} = 1.481V \tag{5}$$

In real operating conditions the actual cell voltage E_{cell} is calculated as a function of operating temperature T_{op}, anodic pressure P_{an} (the pressure at the electrode where the H_2 is being produced) and current density j by modelling the open circuit cell voltage E_{cell}^{OC}. This is done using the Nernst equation and the three main Over Potentials (OP) affecting the voltage under kinetic conditions when a current is applied (Equation (6)):

(i) Activation OP, V_{act} caused by the needed extra potential to overcome the activation energy of the reaction [30,56,59,61],
(ii) Ohmic OP, V_{ohm} caused by the circulation of electrons and protons through resistive media [30,31,56],
(iii) Concentration or Diffusion OP, V_{diff} caused by the effect of gas diffusion in the electrode porous media [30,56,59,61].

$$E_{cell} = E_{cell}^{OC}(T_{op}, P_{an}) + V_{act}(T_{op}, j) + V_{ohm}(T_{op}, j) + V_{diff}(T_{op}, j) \tag{6}$$

The j vs. E_{cell} curve, namely polarization curve, obtained from the model is presented in Fig. 3, together with the impact of each OP term where it can be seen that the main OP contribution is the activation potential. The cell voltage varies in a range from 1.6 to 2.3 V for current densities between 0.1 and 1.6 A/cm^2 in line with results seen in literature [62–66].

The polarization curve allows to obtain the voltage efficiency curve as a function of the current density, which is a function of the operating conditions of the cell as shown in Fig. 4 (function of temperature) and Fig. 5 (function of pressure). It can be see that the voltage efficiency of the cell increases with increasing cell operating temperature and decreases with increasing H_2 pressure for the ranges close to the nominal operating conditions ($T_{op} = 80\,^{\circ}C$; $P_{an} = 20\,bar$) in line with trends found in literature [65–67]. One important fact is that the voltage efficiency of the cell, hence the cell efficiency, increases with lower current density in the cell while Faraday efficiency is assumed constant, thus, the stack efficiency is not maximized at nominal current.

PEM stack model

The PEM stack hereby considered [68] is constituted by 102 cells connected in series, so the stack voltage is given by the sum of the voltage cells (each assumed to operate at equal voltage). The cell interconnection losses are neglected and the PEM stack nominal power is 220 kW. The stack input power P_{stack}^{in} (Equation (7)) is therefore calculated as a function of the stack current (which is the same for each cell, connected in series) and cell voltage obtained at the operating conditions of the cell (T_{op}, P_{an}). The design parameters are: (i) A_{cell}^{active} cell active area and (ii) $N_{\frac{cells}{stack}}$ number of cells per stack.

Table 5 – PEM capacity (MWac) for each DC/AC ratio and each AC/AC ratio.

	AC/AC ratio				
DC/AC	1.0	1.2	1.4	1.6	2.0
1.0	25.6	22.2	18.9	15.5	12.1
1.1	24.3	21.1	17.9	14.7	11.5
1.2	23.0	20.0	17.0	13.9	10.9
1.3	21.8	18.9	16.0	13.2	10.3
1.4	20.5	17.8	15.1	12.4	9.7
1.5	19.2	16.7	14.1	11.6	9.1
1.6	17.9	15.6	13.2	10.8	8.5
1.7	16.6	14.5	12.3	10.1	7.9
1.8	15.4	13.3	11.3	9.3	7.3
1.9	14.1	12.2	10.4	85.2	6.7
2.0	12.8	11.1	9.4	7.7	6.1

Table 6 – Economic parameters and financial assumptions.

Cost	Item	Current	Unit
Specific CAPEX	PV modules	0.4	USD/W_{dc}
	Solar BoP	0.1	USD/W_{dc}
	Solar development (cost & margin)	0.1	USD/W_{dc}
	Grid-forming Inverter	0.07	USD/W_{ac}
	Electrolysis PEM plant	1.2	USD/W_{ac}
	PEM development (cost & margin)	0.5	USD/W_{ac}
Specific OPEX	O&M Solar	0.04	USD/W_{dc}/year
	O&M Electrolyzer (2% CAPEX)	0.024	USD/W_{ac}/year
	Tap water cost	2	USD/m^3
Project finance assumptions	WACC (i)	7	%
	Project horizon (T)	20	years

$$P_{stack}^{in} = \left(E_{cell} \cdot j \cdot A_{cell}^{active}\right) N_{\frac{cells}{stack}} \tag{7}$$

with expressions for input power and stack efficiency available, the H_2 mass flow rate can be obtained by considering the High Heating Value (HHV) of H_2 (285 kJ/mol or 141.8 MJ/kg) [59] as shown in Equation (8).

$$\dot{m}_{H_2}^{real} = \frac{P_{stack}^{in} \cdot \varepsilon_V \cdot \varepsilon_F}{HHV} = N_{\frac{cells}{stack}} \cdot \frac{I_{cell}}{nF} \cdot \varepsilon_F \tag{8}$$

BoP model

The BoP is modelled as modular and the number of BoP modules is equal to the number of PEM stacks. It includes rectifier & power-electronic loads, water pumping and treatment, cooling systems, H_2 purification systems, safety, control and lighting loads, adding an average around 16% of power requirement to the stack capacity depending on the operational point in line with literature [69]. The water treatment includes demineralization and de-ionification of tap water with an assumed efficiency of 1.6 $L_{tap,\ water}/L_{demi,\ water}$, apt for the electrolysis process, leading to an estimated total tap water consumption of 16 [L/kgH_2] in line with stoichiometric water consumption and water purification system efficiencies reported in literature [70].

Black box system model

In order to obtain a simplified model, functional to perform multiyear simulations with hourly resolution with less computational time, a second step to simplify the model was taken. A black-box model with a dynamic efficiency dependent on the power input only was developed. This was modelled starting from the output of the presented parametric model by setting the H_2 outlet pressure at 20 bars and the stack operating temperature at 80 °C. These operational parameters are assumed to be ensured at all times with the support of the BoP. In addition, the system is restricted to operate between [10%–100%] of its nominal capacity. The simplified model is presented in the following Figs. 6 and 7.

It can be seen that while the specific consumption of the stack increases with higher power input due to lower voltage efficiency, the BoP consumption (formed mainly by resistive loads and pumps) converges to its optimal close to the nominal power input or equivalently 1 per unit (1 [p.u.]). The addition of these two consumptions of opposite trends results in the total system specific energy consumption, which is used in the simulator. To do that, the black box system efficiency is modelled for nominal operational conditions as a one-dimensional polynomial fit of order 10 (Equation (9)), of the obtained total efficiency curve. This polynomial fit, minimizes the squared error obtaining a Pearson Correlation Coefficient (R) of 0.998 compared to the parametric result as shown in Fig. 8 and it is a function of the normalized power input only as shown in the equation below. As seen in Fig. 8, the specific consumption converges for power inputs larger to 50% of the nominal capacity to a value around 58 [kWh/kgH2] for the stack and around 67 [kWh/kgH2] for the whole system in line with literature and commercial provider claims [71–73].

$$\varepsilon_{blackbox\left(x=\frac{P_{in}}{P_{nom}}\right)}^{system} = \sum_{k=0}^{n=10} x^{n-k} \cdot c_k \tag{9}$$

where:

$c_0 = 1.2852e{+}05$ $c_6 = 1.9732e{+}06$,
$c_1 = -9.2233e{+}05$ $c_7 = -6.0915e{+}05$
$c_2 = 2.8742e{+}06$ $c_8 = 1.1617e{+}05$
$c_3 = -5.1006e{+}06$ $c_9 = -1.2504e{+}04$
$c_4 = 5.6818e{+}06$ $c_{10} = 6.7535e{+}02$
$c_5 = -4.1299e{+}06$

Table 7 – PEM cell and system characteristics assumed for the model [55].

Parameter	value
Operating pressure	0–30 bar
Operating temperature	80 °C
Total plate area	957 cm^2
Single cell active area	680 cm^2
Nominal current density	1.7 A/cm^2

Economic modelling

The economic analysis of the model output data is done performing a classic project financial assessment on the base of the expected cash flows linked to the project investment under a conventional project finance structure and to its operational expenses. This analysis is carried separately for the solar system alone first and for the complete system including the electrolysis plant after. This allows comparing

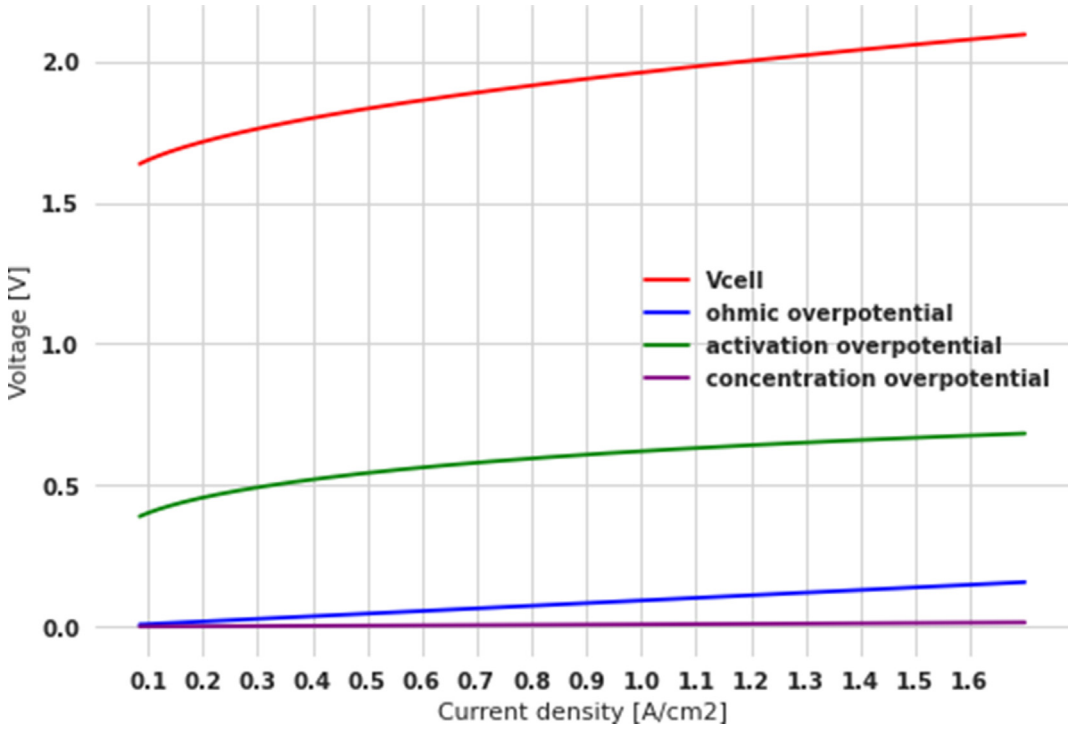

Fig. 3 – Polarization curve from the model at cell level.

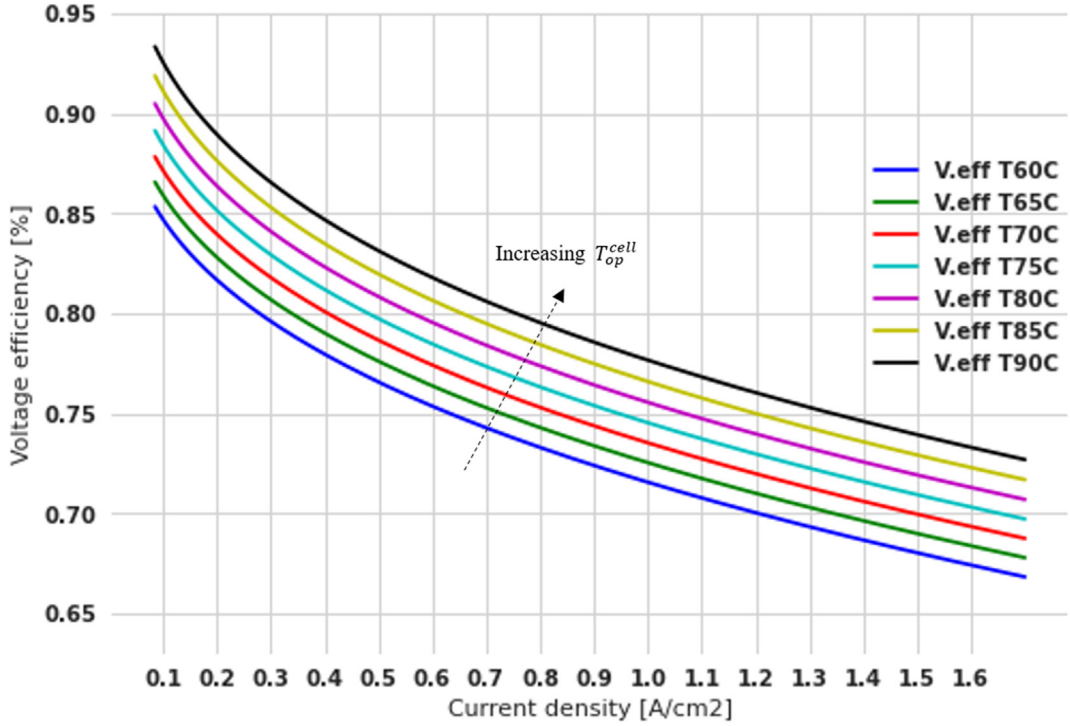

Fig. 4 – Voltage efficiency output as a function of cell operating temperature.

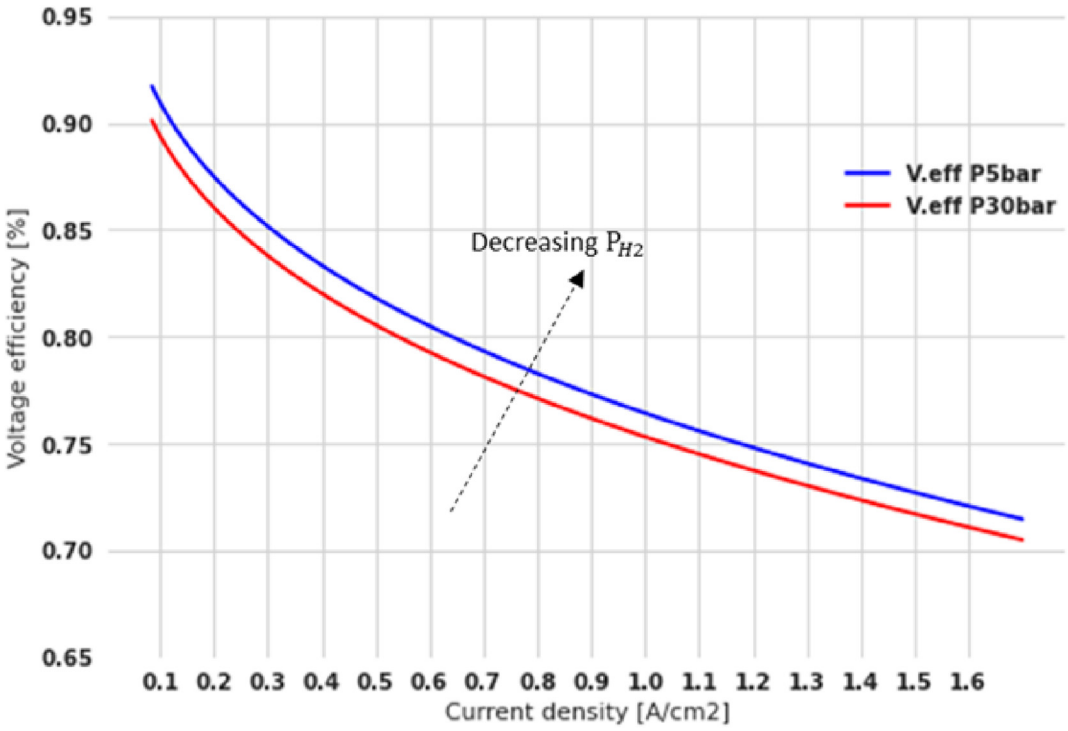

Fig. 5 – Voltage efficiency output as a function of operating H_2 outlet pressure.

the optimality of the solar design when the aim is to produce energy only versus producing hydrogen. The considered expressions for NPV, LCOE and LCOH are listed in following Equations (10)–(12). The values within the summations are all yearly values and rates.

$$NPV_{costs_X} = CAPEX_X + \sum_{t=1}^{T} \frac{OPEX_{X(t)}}{(1+i)^t} \tag{10}$$

$$Solar\ LCOE = \frac{NPV_{costs\ \ Solar}}{\sum_{t=1}^{T} \frac{Energy\ output_{(t)}}{(1+i)^t}} \tag{11}$$

$$LCOH = \frac{NPV_{costsTotal\ \ system}}{\sum_{t=1}^{T} \frac{H_{2(t)}}{(1+i)^t}} \tag{12}$$

The optimization in this study is based on the minimization of LCOH as a function of the DC/AC and AC/AC ratio for a given PV capacity, therefore the updating variable in the optimization process are the power capacity of the solar inverter and electrolyzer respectively as shown below:

$$\min\ LCOH\left(P^{out}_{inverter}, P^{in}_{electrolyzer}\right) \tag{13}$$

The LCOH is obtained by post processing the results for each configuration defined by the sizing ratios keeping the solar PV capacity fixed. The operation of each configuration is simulated with hourly resolution for 20 years and the spectrum of configurations is covered with an iterative algorithm that then finds the min-LCOH configuration.

Results and discussion

Solar system performance

The first results assessed are the performance of the solar systems under different configurations and locations.

Fig. 6 – Black box model PEM electrolysis system.

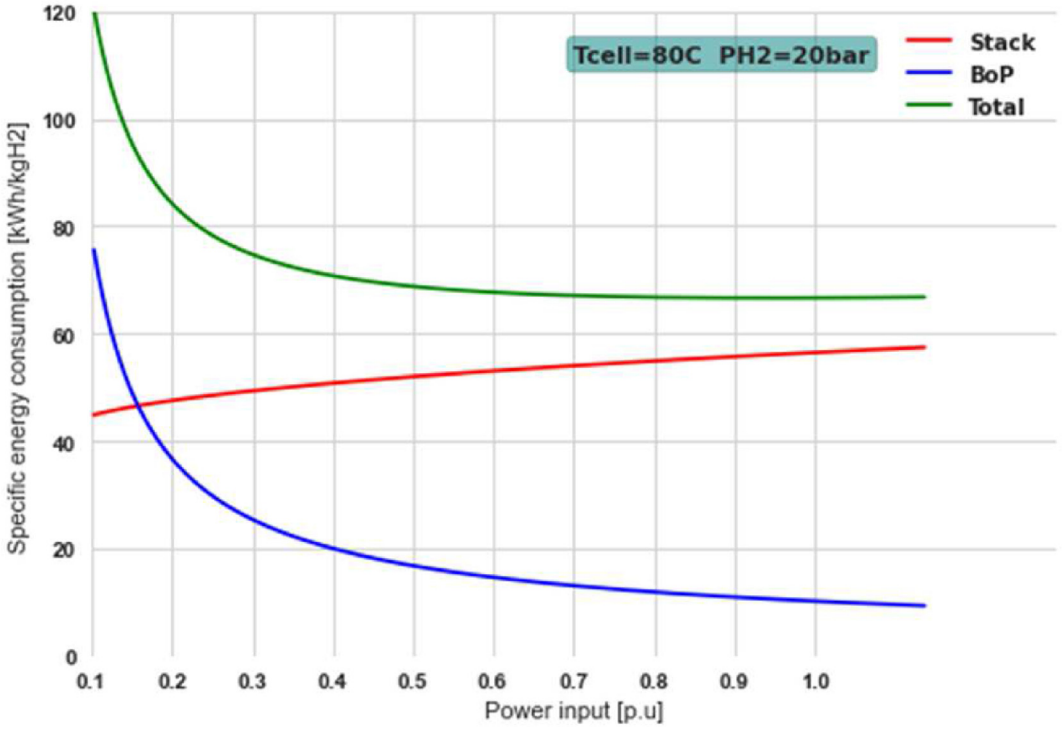

Fig. 7 – Black-box system specific consumption as a function of input power.

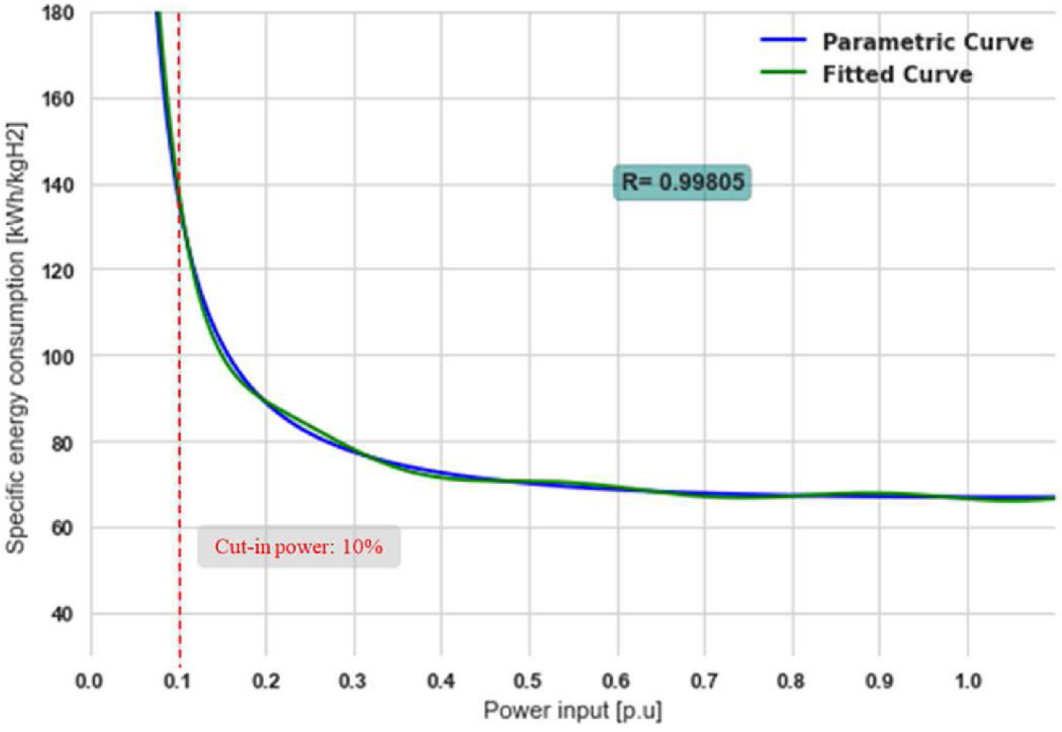

Fig. 8 – System efficiency polynomial fit.

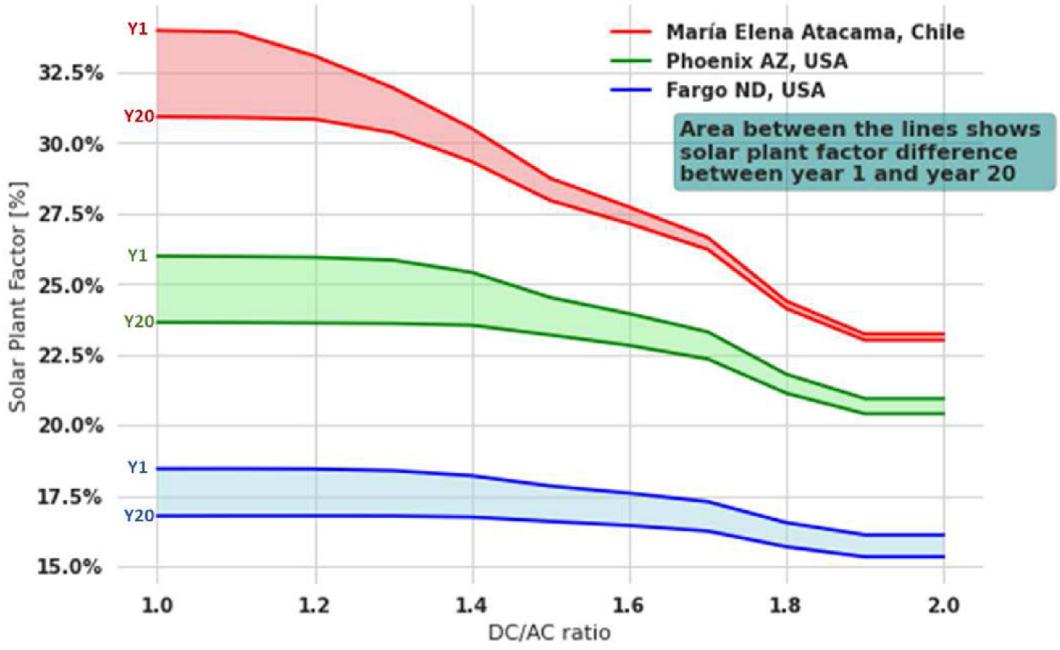

Fig. 9 – Solar system plant factor and degradation effect.

Naturally, as shown in Fig. 9, the plant factor of the solar system, which is a metric given by the production of the system normalized by its installed capacity also known as capacity factor, is strongly dependent on the location and solar resource. Also as expected, the dependence of the solar plant factor with respect to the DC/AC is stronger for locations with higher GHI as Atacama compared to locations with low GHI as North Dakota. For all three locations, there are clear maxima and minima plant factors with respect to the DC/AC ratio. However, these are obtained at different DC/AC ratios depending on the location. For higher GHI, DC/AC ratio that maximizes plant factor is small, close to one which means a large inverter, while the minimum plant factor is reached at very large DC/AC ratios. On the other hand, if the solar resource is low, the plant factor is already close to its maximum even with small inverter capacity or large DC/AC ratio as seen in the case of North Dakota.

The degradation effect on the solar plant, shown in the same figure as the area between the same colour curves, is a function of both the location and the DC/AC ratio. In particular, for small DC/AC ratios such as one (inverter capacity as large as PV capacity), the degradation effect is more accentuated in locations with high GHI due to the fact that the inverter is converting all the DC output from the PV modules which are the most affected by degradation. For larger DC/AC ratios such as two, the degradation affects the plant factor more in locations with low GHI. This is because small inverter capacities cannot take in all the input from the PV system and operate from the beginning of the project life with DC curtailment. If the GHI is high the DC curtailment is large and the PV module degradation will affect the portion of DC generation being curtailed, thus, allowing the solar system to continue operate close to full capacity even when the PV modules are affected by degradation.

To understand better the effects of curtailment and seasonality, the weekly performance of two solar plant configurations, one with large inverter capacity (DC/AC = 1.2) and one with small inverter capacity (DC/AC ratio = 1.8), are shown in the following figures. The 4 days plotted correspond to summer and winter solstice weeks. The plots show the performance of the plants in the three locations considered: North Dakota, Arizona, and Atacama in Figs. 10, 11 and 12 respectively. The yellow area represents the DC power output from the PV modules while the green and red dashed lines denote the hourly output of the plant with large and small inverter capacity respectively. Notice that summer and winter solstice correspond to June and December respectively for locations in USA while for Chile is the opposite.

Curtailment can be identified in the plots when a flat plateau is reached in the AC output lines despite the available surplus of DC power seen above the plateau. In particular, for North Dakota (low radiation) it can be seen that during winter there is no curtailment of DC power output for both DC/AC ratios of 1.2 and 1.8. That means that the nominal capacity of the inverter in both cases was not surpassed by the DC input coming from the solar field. During summer, there are only a few hours of the solstice where curtailment is observed for DC/AC of 1.8 in the same location.

On the other hand for Atacama (high radiation) a large portion of the solar DC output is curtailed for both configurations during summer and winter, making the annual plant factor quite sensitive to the size of the inverter thus to the DC/AC ratio. For Arizona (medium radiation) there is curtailment only in summer and it is less pronounced than in Atacama.

The figures above show how the solar electricity production is less sensitive with respect to DC/AC ratios in locations with low radiation and much more sensitive (or elastic) for

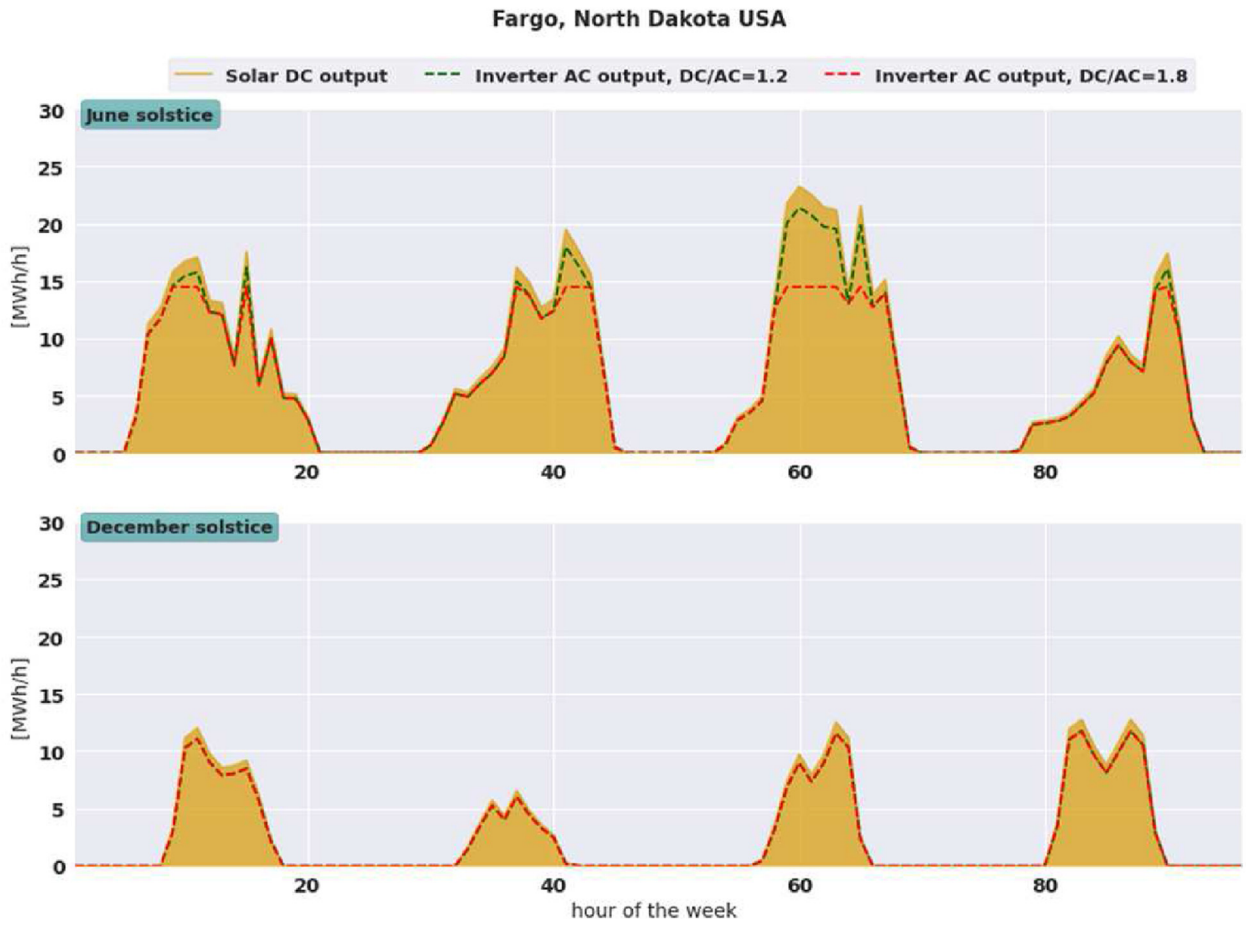

Fig. 10 – Performance of solar power plants during summer solstice week (top) and winter solstice week (bottom) – Fargo.

places with high radiation with respect to the same variable. In summary, for locations with high annual GHI such as Atacama, a larger DC/AC ratio implies curtailment (even in winter) so the inverter capacity maximizing production will tend to be larger (small DC/AC ratio). Locations with lower GHI such as North Dakota, large inverters do not imply more production due to low utilization factor thus larger DC/AC ratios can be use without losing production.

Solar system economic performance

In a system meant to produce electricity only, a common optimization metric is the LCOE. The results above showed how location and DC/AC ratio affect production, however the LCOE metric takes into account also the costs of developing and operating the solar system. In Fig. 13 the LCOE obtained for our three case studies, its dependency of DC/AC ratio, and the DC/AC ratio that optimizes LCOE for each location are shown.

As expected, for locations with higher GHI, a lower LCOE is obtained due to higher utilization factor and vice-versa. An important consequence of this is that for higher GHI, the optimal LCOE is obtained at lower DC/AC ratios (1.1 in Atacama) than for lower GHI (1.2 and 1.3 in North Dakota and Arizona respectively). Despite the existence of an optimal LCOE, its value do not vary largely within the same location. Unlike the plant factor, the LCOE behaves quite inelastic to changes in the DC/AC ratio when close to the optimal DC/AC ratio.

Solar hydrogen results

After reviewing the solar energy production results, the hydrogen production and economic performance of the complete system can be studied. Figs. 14, 15 and 16 show the hydrogen production at the three locations for DC/AC ratios of 1.2 and AC/AC ratios of 1.8, 1.5 and 1.3 for North Dakota, Arizona and Atacama respectively.

In the case of North Dakota, location with low GHI, results for a large AC/AC ratio close to two are shown. Even with this configuration with an electrolyzer undersized compared to the solar inverter, there is no AC power curtailment during winter. The overall oversizing of the PV installed capacity compared to the electrolyzer is equal to 1.2 time 1.8, with a total oversizing factor of 2.16.

For Arizona, results for an AC/AC ratio of 1.5 are shown where curtailment is perceived during summer but not in winter. On the other hand, in Atacama, where the load factor is much higher due to higher GHI, even with an AC/AC ratio of 1.3 there is considerable curtailment in summer.

The dependency patterns of hydrogen production with respect to AC/AC for the different locations appears to be similar to what it is observed for the solar inverter AC energy production and its dependency of DC/AC ratio for solar plants. However, in order to understand the implications of considering the AC/AC ratio for optimal sizing the economic factors should be taken into account as presented in the following subsection 5.4.

Solar hydrogen economic performance

The total cost of development and operation of these systems is constituted by CAPEX and OPEX. Since OPEX is spent during the lifetime, in order to understand the Total Expenditures (TOTEX), it is useful to look at the Net Present Value (NPV) of the TOTEX. Fig. 17 shows this metric for all configurations. Notice that for this study, the TOTEX is the same for all three locations as the same specific CAPEX and OPEX was considered in all three cases for both solar and electrolysis technologies (even if their electricity and/or hydrogen production is different). As expected, the larger the ratios, the higher the TOTEX varying quite sharply. Without under sizing (both sizing ratios = 1) the TOTEX reaches 80.5 MMUSD while for a configuration with ratios of 2 it reaches 41.9 MMUSD.

From a pure cost perspective, it is desirable to have lower TOTEX, therefore larger sizing ratios or small downstream assets compared to the solar field. However, this has to be contrasted with production data for each configuration via a pertinent metric such as LCOH to allow concluding about economic optimality of the configuration, as a more expensive project in terms of TOTEX could still lead to an optimal configuration if the hydrogen production is large enough to justify the investment and operational expenses.

Fig. 18 shows H_2 production per configuration, per location, during the first year of operation. Unlike TOTEX, H_2 production is not only a function of configuration and size but also location.

Locations with low GHI present lower H_2 production than locations with higher GHI for all configurations as expected while for all three locations, larger ratios imply a reduction in the total output.

For Atacama (high GHI), the output difference between the least undersized (sizing ratios = 1) and the most undersized case (sizing ratios = 2) is as large as 185% (1192–417 tons H_2/year) whereas for Arizona and North Dakota the same variation reaches values of 126% (896-392 ton H_2/year) and 69% (596-352 ton H_2/year) respectively. This shows that the hydrogen output sensitivity with respect to sizing ratios is stronger in locations with higher radiation. In other words, for low radiation locations, the hydrogen production will not vary

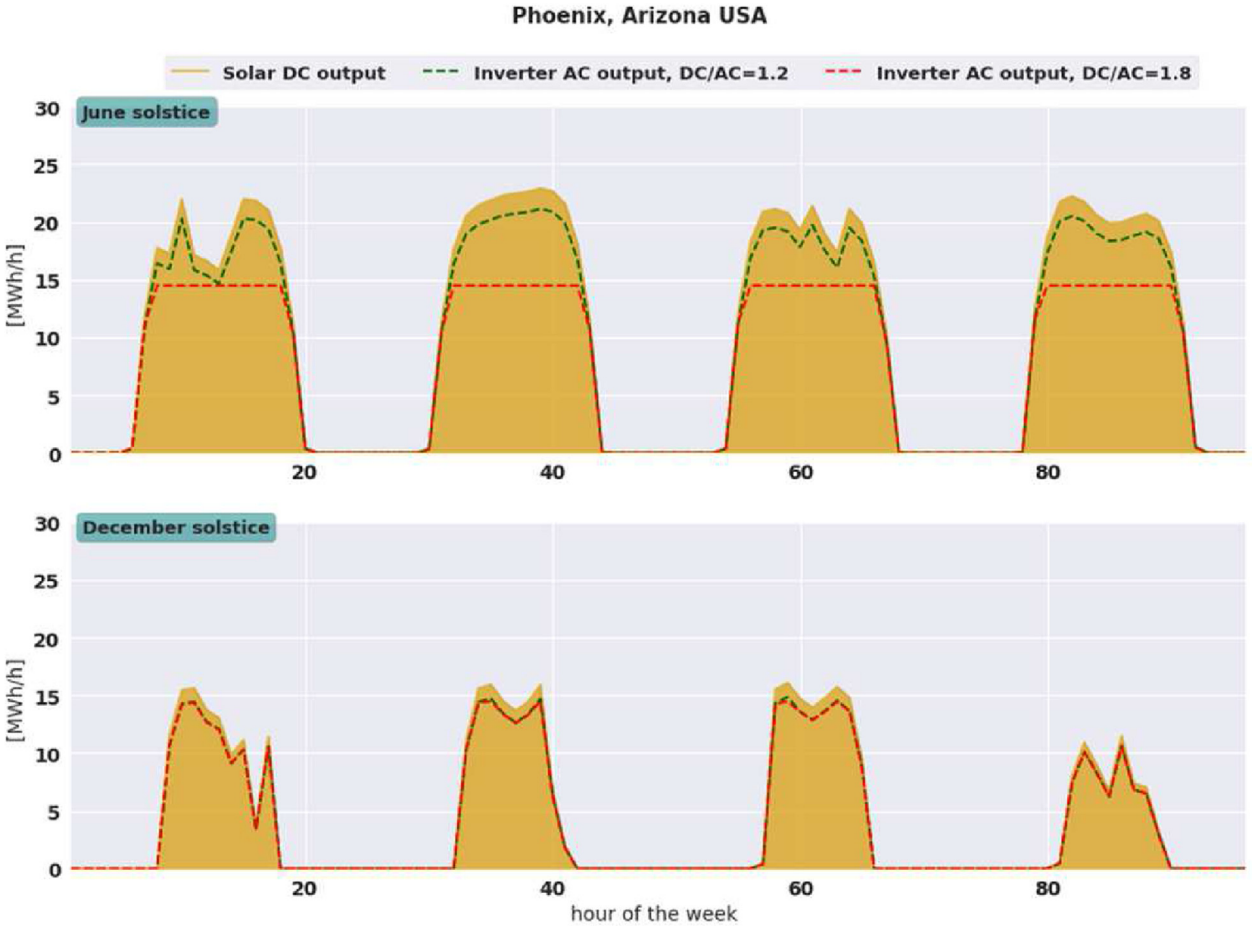

Fig. 11 – Performance of solar power plants during summer solstice week (top) and winter solstice week (bottom) – Phoenix.

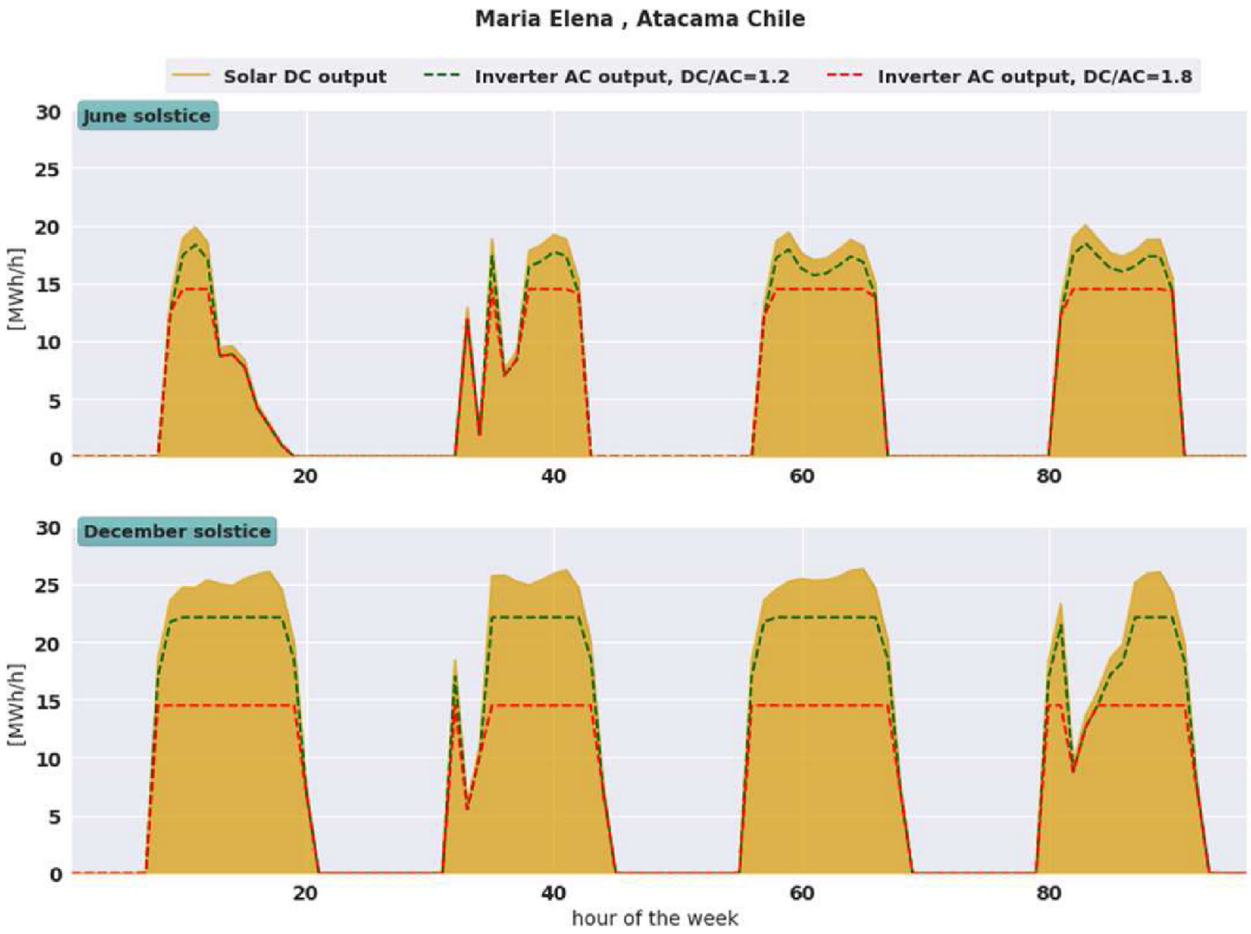

Fig. 12 – Performance of solar power plants during winter solstice week (top) and summer solstice week (bottom) - Ma. Elena.

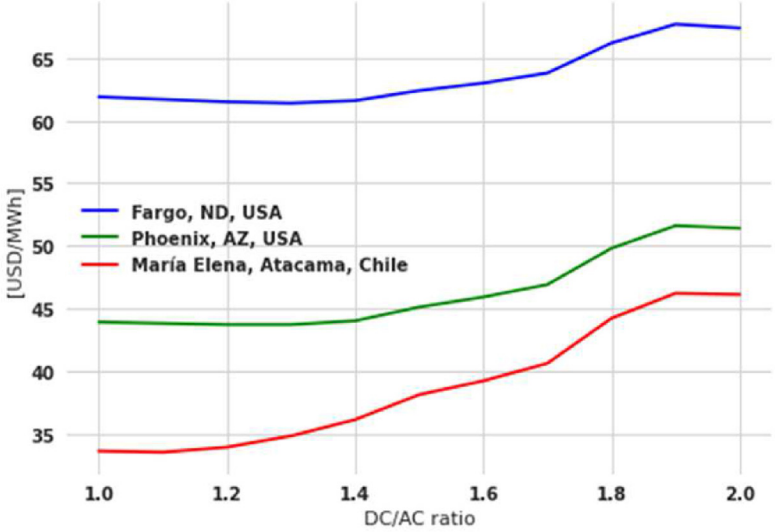

Fargo, USA	61.9	61.7	61.5	Min 61.4	61.6	62.4	63.0	63.8	66.2	67.7	67.4
Phoenix, USA	43.9	43.8	Min 43.7	43.7	44.0	45.1	45.9	46.9	49.8	51.6	51.4
M.Elena, Chile	33.6	Min 33.5	33.9	34.8	36.1	38.1	39.2	40.6	44.2	46.2	46.1

Fig. 13 – Solar plant's LCOE as a function of DC/AC ratios and location.

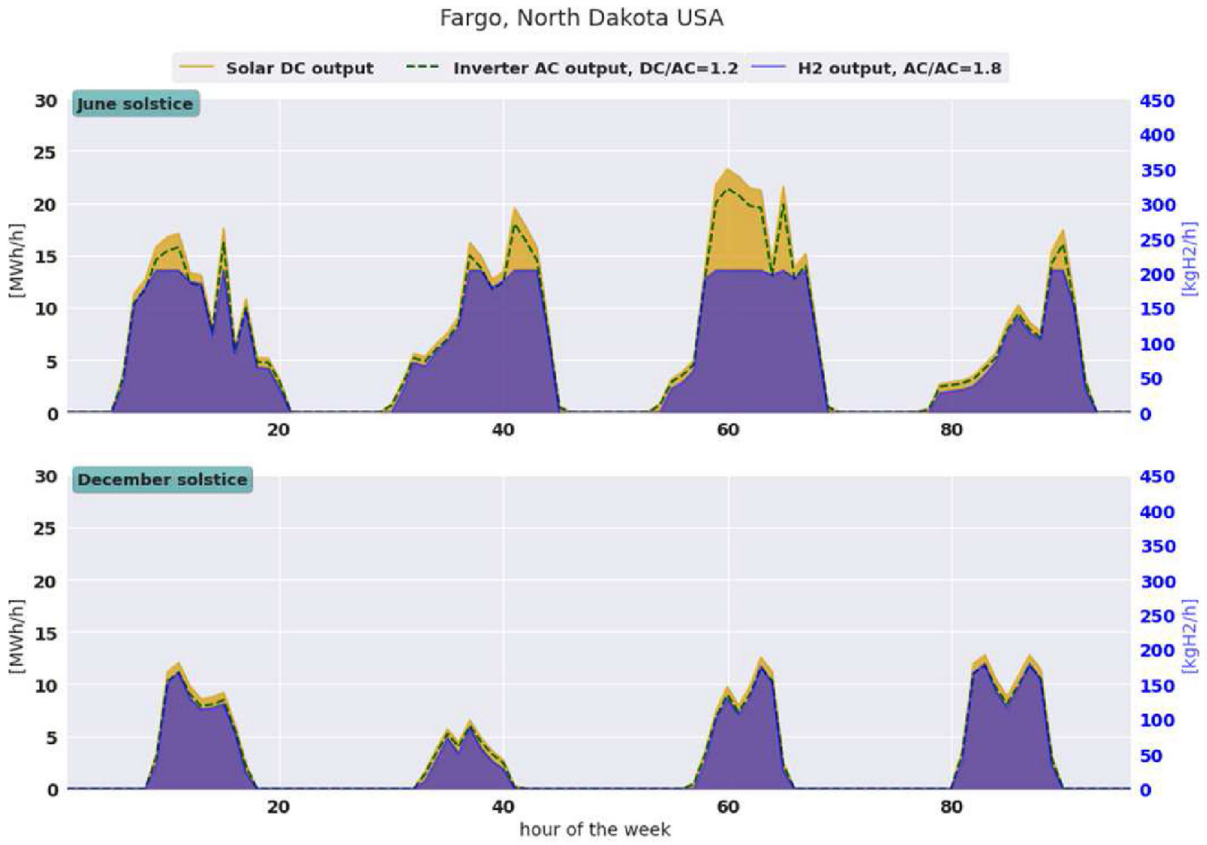

Fig. 14 – Hydrogen production during summer solstice week (top) and winter solstice week (bottom) – Fargo, North Dakota.

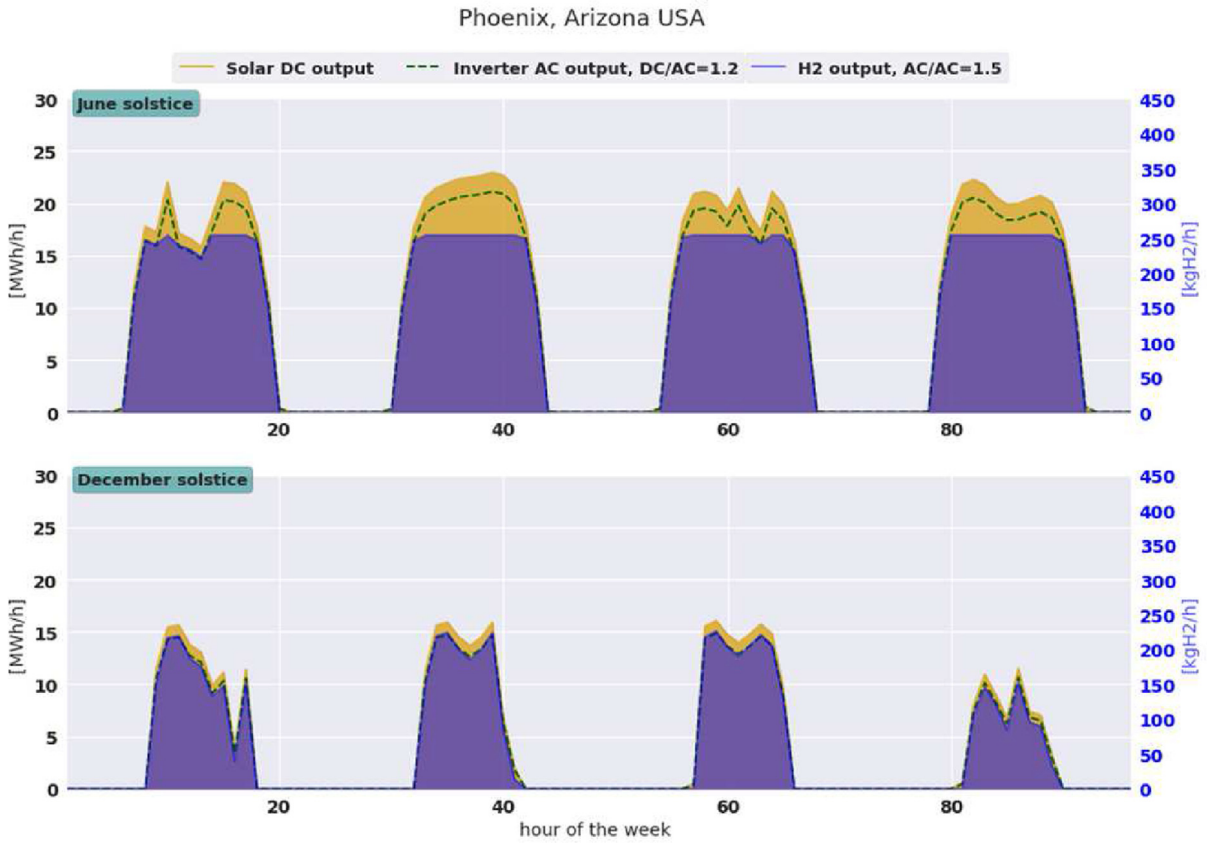

Fig. 15 – Hydrogen production during summer solstice week (top) and winter solstice week (bottom) – Phoenix.

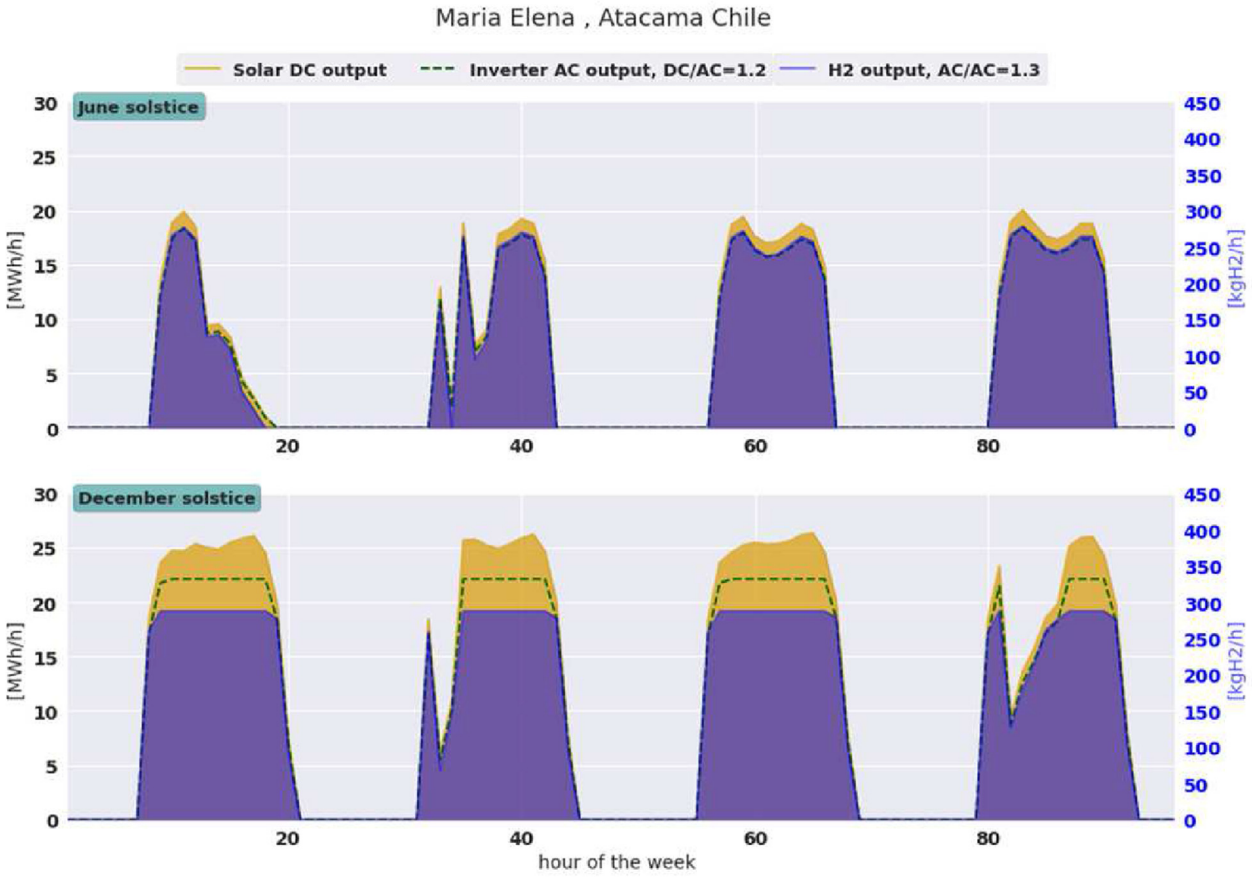

Fig. 16 – Hydrogen production during winter solstice week (top) and summer solstice week (bottom) - M. Elena, Atacama.

strongly for undersized electrolyzers whereas for high radiation locations, undersizing the electrolyzer compared to the solar system can imply large output loss.

Unlike the case of TOTEX, from a pure production perspective, it is desirable to maximize the H_2 output, therefore smaller sizing ratios or large downstream assets compared to the solar field are required. In order to contrast both drivers, we examine the LCOH metric, which combines both TOTEX and H_2 production per configuration allowing to identify the most competitive configuration overall. The LCOH results for each configuration in each location combining the data of cost and production are shown in Fig. 19.

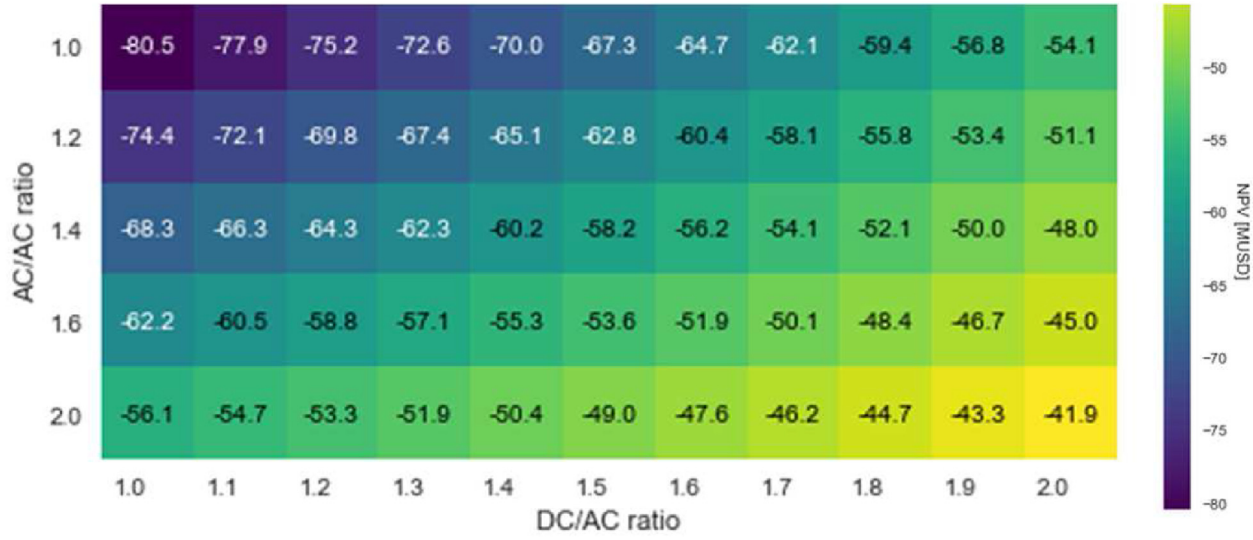

Fig. 17 – Net Present Value of Total Expenditures per configuration.

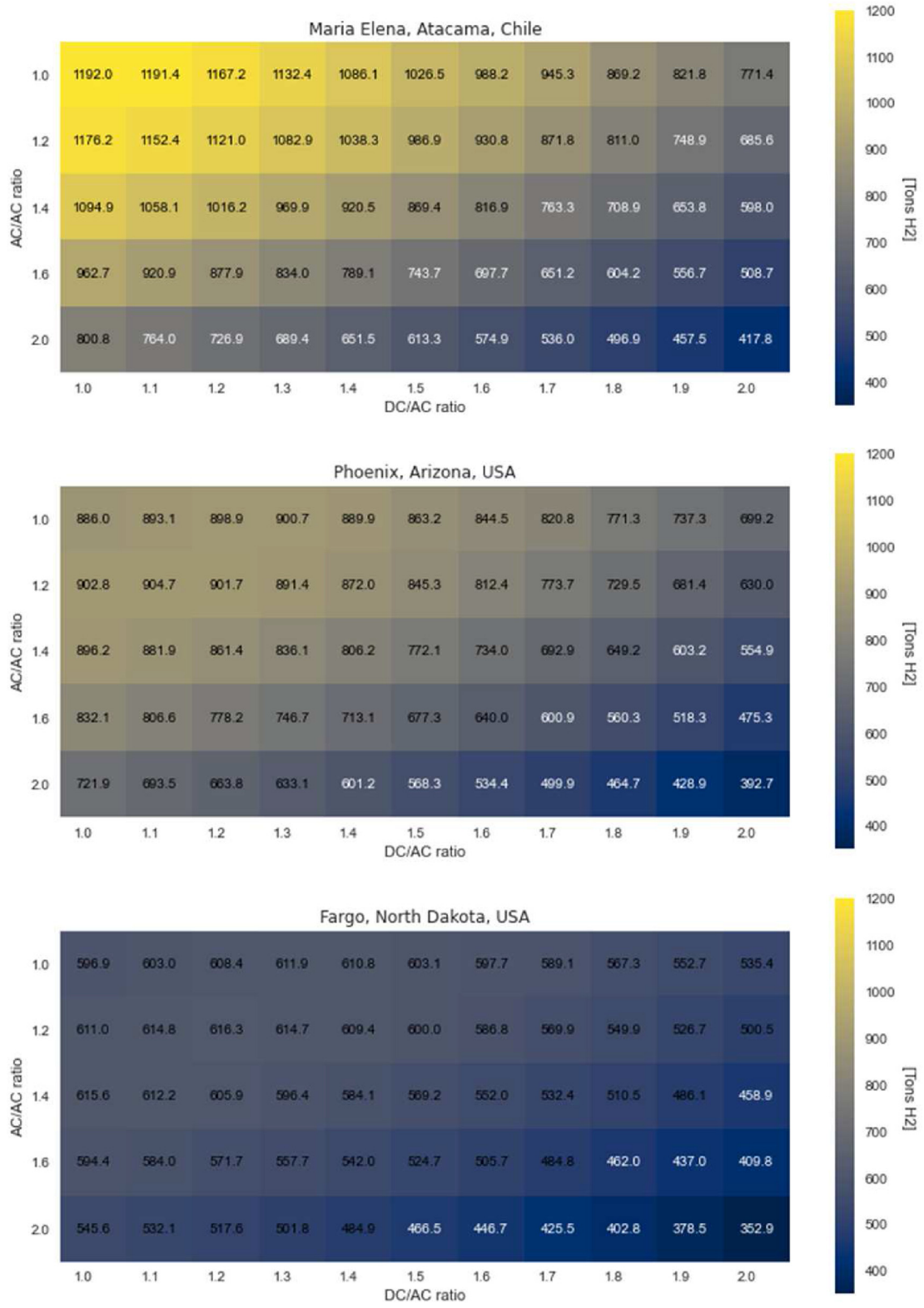

Fig. 18 – Hydrogen production (first year) for different AC/AC ratios and DC/AC ratios for Ma. Elena (top), Phoenix (centre) and Fargo (bottom).

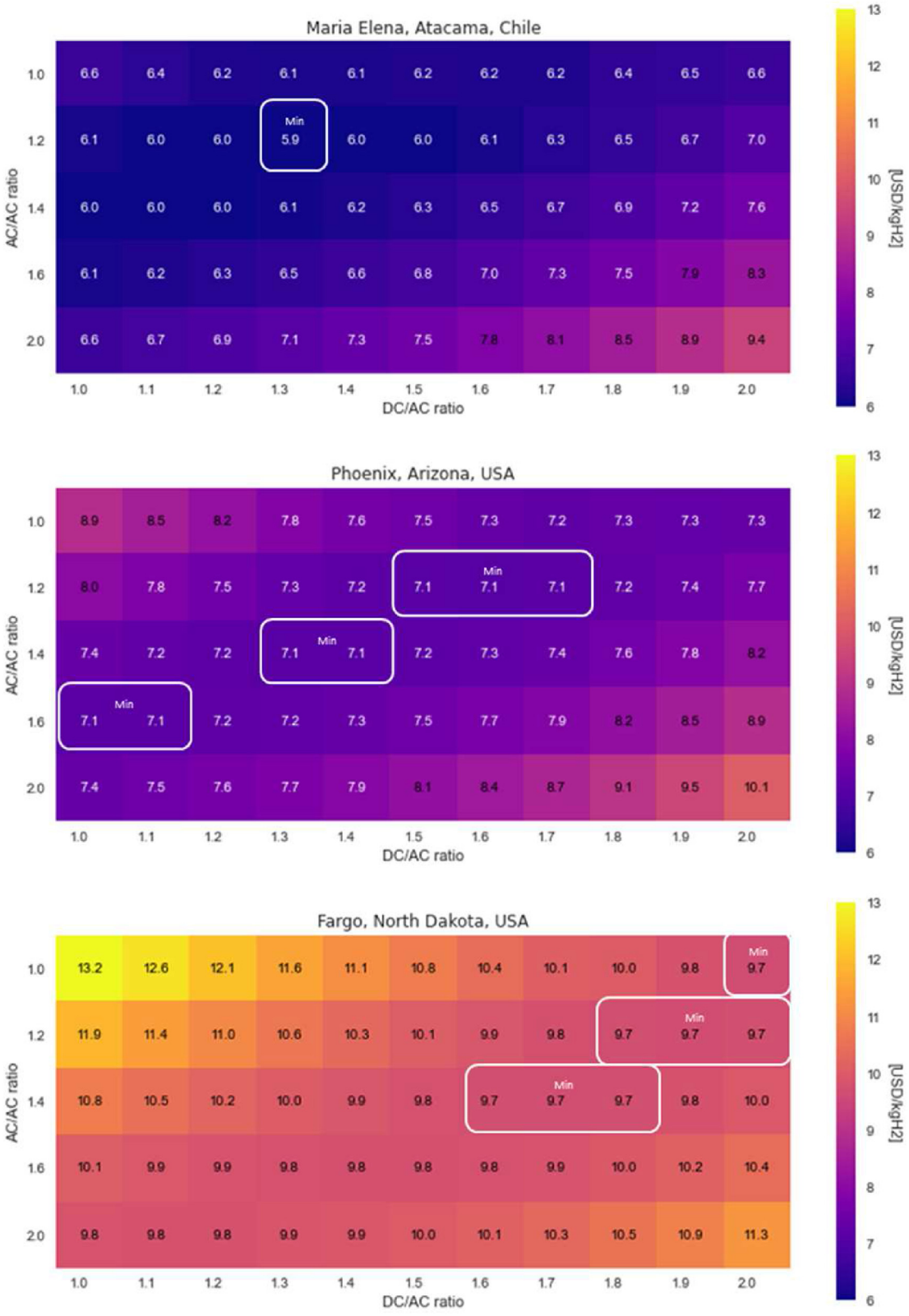

Fig. 19 – Levelized Cost of Hydrogen LCOH for different AC/AC ratios and DC/AC ratios for Ma. Elena (top), Phoenix (centre) and Fargo (bottom).

In the case of LCOH as a function of sizing ratios, unlike figures of cost-only or H_2-production-only, the minimum values are not located in the extremes nor corners of the heat map. The minimum LCOH is actually reached within the envelope of the spectrum and not in the contour of the studied spectrum.

The optimal LCOH presents different patterns depending on the location. As expected, it is in general lower for Atacama than for Arizona, and lower for Arizona than for North Dakota due to the difference in the solar resource.

In Atacama, the min-LCOH is 5.9 USD/kgH_2 obtained with a configuration of DC/AC = 1.3 and AC/AC = 1.2. This configuration leads to a total production of 1082 tons H_2/year. The LCOH does not vary greatly for similar configurations with sizing factors near the minima with LCOHs close to 6 USD/kgH_2 however it increases sharply for larger sizing ratios reaching 9.4 USD/kgH_2 (bottom right corner of the heat map). It should be noticed that for Atacama the optimal DC/AC ratio of the solar plant for min-LCOH is 1.3, different from the 1.1 obtained for min-LCOE of the solar plant. Furthermore, DC/AC ratios as large as 1.5 can led to close to min-LCOH levels for AC/AC ratios close to 1.2.

For Arizona, there is no a unique configuration leading to a min-LCOH. The min-LCOH of 7.1 USD/kgH_2 is obtained for several configurations. In particular, it can be obtained for an AC/AC ratio of 1.2 and DC/AC ratios between [1.5–1.7] and even for an AC/AC ratio as large as 1.6, if keeping the DC/AC ratio between [1–1.1]. Depending on the strategy, access to capital and production needs, the optimal DC/AC ratio can range between [1–1.7], strongly varying compared to the DC/AC ratio for min-LCOE of [1.2–1.3]. Different optimal LCOH configurations can be designed to deliver between 773 and 832 tons H_2/year for the solar installed capacity of 27 MW with TOTEX varying from 58 to 62 MUSD. Moreover, there are several additional configurations close to these sizing ratios where the LCOH does go vary greatly.

For North Dakota, the LCOH is in general more expensive than for other locations. The min-LCOH is 9.7 USD/kgH_2 for a configuration with larger ratios of DC/AC [1.6–2] and AC/AC [1–1.4] respectively, which means that optimal sizes of inverter and electrolyzer are much smaller than the solar field. The sensitivity of the LCOH with respect to the sizing ratios, appears to be less than for the case of Atacama or Phoenix with a total LCOH range of [9.7–13.2] USD/kgH_2 for the assessed spectrum. The DC/AC that minimizes LCOH is 54% larger than the one that minimizes solar electricity for the same location.

Discussion

For all three results, the effect of the AC/AC ratio is quantified and its impact on LCOH for different radiation levels is observed.

When sizing the subsystems of a solar-electrolysis plant, if optimized separately (not as part of the same system) sub-optimal results are reached for the integrated system. In particular, if the solar system is sized considering min-LCOE, the optimal DC/AC is lower than the one obtained for min-LCOH, especially for locations with low solar GHI, or a larger inverter capacity is chosen. This effect might be compensated to a certain extent by varying the AC/AC ratio to reach optimal LCOH values but resulting in a more restricted spectrum of configurations for the electrolyzer.

The optimal sizing ratios could be selected considering several criteria dependent of each stakeholder where factors such as H_2 production volume needs or access to and cost of capital, which are both a function of the sizing ratios and project location, can play an important role.

Conclusions

In this study, a model for off-grid PV-PEM for H_2 production systems and a methodology to investigate the optimal configuration of such plant are proposed. The optimal sizing is location dependent.

Optimal LCOH values can be obtained for different plant configurations, which in this study were defined by combinations of DC/AC and AC/AC ratios. For a given location, these configurations lead to different TOTEX and H_2 annual production even for very close ranges of LCOH values.

The AC/AC ratio should be taken into consideration as a design variable when optimizing the size of these plants. The novelty of this study is to propose a definition for this metric and a straightforward methodology to assess its impact in terms of H_2 production, CAPEX and LCOH for different locations covering a range of solar radiation conditions.

Limitations of this study include the lack of consideration of additional downstream assets such as storage technologies as well as considering demand, handling and use phase of the hydrogen or its derivatives. These factors will be investigated in future work.

Funding

This work is part of the project "Circular Techno-Economic Analysis of Energy Storage & IEA co-coordination" funded by the Swedish Energy Agency "*Energimyndigheten*".

Declaration of competing interest

The authors declare that they have no known competing financial interests or personal relationships that could have appeared to influence the work reported in this paper.

REFERENCES

[1] IEA. The future of hydrogen. IEA; 2019.
[2] Kakoulaki G, Kougias I, Taylor N, Dolci F, Moya J, Jäger-Waldau A. Green hydrogen in Europe – a regional assessment: substituting existing production with electrolysis powered by renewables. Energy Convers Manag 2021;228:113649. https://doi.org/10.1016/j.enconman.2020.113649.

[3] Hydrogen economy outlook | full report. BloombergNEF 2020. https://www.bnef.com/insights/22567 (accessed January 18, 2022).
[4] Global OECD. Hydrogen review 2021. Paris: Organisation for Economic Co-operation and Development; 2021.
[5] Kyriakopoulos GL, Arabatzis G. Electrical energy storage systems in electricity generation: energy policies, innovative technologies, and regulatory regimes. Renew Sustain Energy Rev 2016;56:1044–67. https://doi.org/10.1016/j.rser.2015.12.046.
[6] Rogelj J, Shindell D, Jiang K, Fifita S, Foster P, Ginzburg V, et al. Mitigation pathways compatible with 1.5°C in the context of sustainable development. In: Masson-Delmotte V, Zhai P, Pörtner H-O, Roberts D, Skea J, Shukla PR, et al., editors. Global Warming of 1.5°C. An IPCC Special Report on the impacts of global warming of 1.5°C above pre-industrial levels and related global greenhouse gas emission pathways, in the context of strengthening the global response to the threat of climate change, sustainable development, and efforts to eradicate poverty. IPCC/WMO; 2018. p. 93–174.
[7] Lazarou S, Vita V, Diamantaki M, Karanikolou-Karra D, Fragoyiannis G, Makridis S, et al. A simulated roadmap of hydrogen technology contribution to climate change mitigation based on Representative Concentration Pathways considerations. Energy Sci Eng 2018;6:116–25. https://doi.org/10.1002/ese3.194.
[8] Streimikiene D, Kyriakopoulos GL, Lekavicius V, Siksnelyte-Butkiene I. Energy poverty and low carbon just energy transition: comparative study in Lithuania and Greece. Soc Indicat Res 2021;158:319–71. https://doi.org/10.1007/s11205-021-02685-9.
[9] The clean hydrogen future has already begun – Analysis. IEA n.d. https://www.iea.org/commentaries/the-clean-hydrogen-future-has-already-begun (accessed January 17, 2022).
[10] International Energy Agency. Global hydrogen review 2021. OECD; 2021. https://doi.org/10.1787/39351842-en.
[11] IEA. In: The Future of Hydrogen; 2019. p. 203.
[12] Pflugmann F, Blasio ND. Geopolitical and market implications of renewable hydrogen. 2020. p. 62.
[13] Geopolitics of the energy transformation: the hydrogen factor n.d.:118.
[14] Pflugmann F, De Blasio N. The geopolitics of renewable hydrogen in low-carbon energy markets. Geopolit Hist Int Relat 2020;12:2374–4383. https://doi.org/10.22381/GHIR12120201.
[15] Gibson TL, Kelly NA. Optimization of solar powered hydrogen production using photovoltaic electrolysis devices. Int J Hydrogen Energy 2008;33:5931–40. https://doi.org/10.1016/j.ijhydene.2008.05.106.
[16] Yang Z, Zhang G, Lin B. Performance evaluation and optimum analysis of a photovoltaic-driven electrolyzer system for hydrogen production. Int J Hydrogen Energy 2015;40:3170–9. https://doi.org/10.1016/j.ijhydene.2015.01.028.
[17] Khalilnejad A, Abbaspour A, Sarwat AI. Multi-level optimization approach for directly coupled photovoltaic-electrolyser system. Int J Hydrogen Energy 2016;41:11884–94. https://doi.org/10.1016/j.ijhydene.2016.05.082.
[18] Sayedin F, Maroufmashat A, Sattari S, Elkamel A, Fowler M. Optimization of Photovoltaic Electrolyzer Hybrid systems; taking into account the effect of climate conditions. Energy Convers Manag 2016;118:438–49. https://doi.org/10.1016/j.enconman.2016.04.021.
[19] Navarro-Solís I, Villalba-Almendra L, Alvarez-Gallegos A. H2 production by PEM electrolysis, assisted by textile effluent treatment and a solar photovoltaic cell. Int J Hydrogen Energy 2010;35:10833–41. https://doi.org/10.1016/j.ijhydene.2010.07.086.
[20] Ferrero D, Santarelli M. Investigation of a novel concept for hydrogen production by PEM water electrolysis integrated with multi-junction solar cells. Energy Convers Manag 2017;148:16–29. https://doi.org/10.1016/j.enconman.2017.05.059.
[21] Paul B, Andrews J. Optimal coupling of PV arrays to PEM electrolysers in solar–hydrogen systems for remote area power supply. Int J Hydrogen Energy 2008;33:490–8. https://doi.org/10.1016/j.ijhydene.2007.10.040.
[22] Shapiro D, Duffy J, Kimble M, Pien M. Solar-powered regenerative PEM electrolyzer/fuel cell system. Sol Energy 2005;79:544–50. https://doi.org/10.1016/j.solener.2004.10.013.
[23] Cai X, Lin R, Xu J, Lu Y. Construction and analysis of photovoltaic directly coupled conditions in PEM electrolyzer. Int J Hydrogen Energy 2021. https://doi.org/10.1016/j.ijhydene.2021.12.017.
[24] Atlam O, Barbir F, Bezmalinovic D. A method for optimal sizing of an electrolyzer directly connected to a PV module. Int J Hydrogen Energy 2011;36:7012. https://doi.org/10.1016/j.ijhydene.2011.03.073. 8.
[25] Grube T, Reul J, Reuß M, Calnan S, Monnerie N, Schlatmann R, et al. A techno-economic perspective on solar-to-hydrogen concepts through 2025. Sustain Energy Fuels 2020;4:5818–34. https://doi.org/10.1039/D0SE00896F.
[26] Reuß M, Reul J, Grube T, Langemann M, Calnan S, Robinius M, et al. Solar hydrogen production: a bottom-up analysis of different photovoltaic–electrolysis pathways. Sustain Energy Fuels 2019;3:801–13. https://doi.org/10.1039/C9SE00007K.
[27] Ceylan C, Devrim Y. Design and simulation of the PV/PEM fuel cell based hybrid energy system using MATLAB/Simulink for greenhouse application. Int J Hydrogen Energy 2021;46:22092–106. https://doi.org/10.1016/j.ijhydene.2021.04.034.
[28] Ghribi D, Khelifa A, Diaf S, Belhamel M. Study of hydrogen production system by using PV solar energy and PEM electrolyser in Algeria. Int J Hydrogen Energy 2013;38:8480–90. https://doi.org/10.1016/j.ijhydene.2012.09.175.
[29] Scamman D, Bustamante H, Hallett S, Newborough M. Off-grid solar-hydrogen generation by passive electrolysis. Int J Hydrogen Energy 2014;39:19855–68. https://doi.org/10.1016/j.ijhydene.2014.10.021.
[30] Aouali FZ, Becherif M, Tabanjat A, Emziane M, Mohammedi K, Krehi S, et al. Modelling and experimental analysis of a PEM electrolyser powered by a solar photovoltaic panel. Energy Proc 2014;62:714–22. https://doi.org/10.1016/j.egypro.2014.12.435.
[31] Khelfaoui N, Djafour A, Ghenai C, Laib I, Danoune MB, Gougui A. Experimental investigation of solar hydrogen production PV/PEM electrolyser performance in the Algerian Sahara regions. Int J Hydrogen Energy 2021;46:30524–38. https://doi.org/10.1016/j.ijhydene.2020.11.193.
[32] Papadopoulos V, Desmet J, Knockaert J, Develder C. Improving the utilization factor of a PEM electrolyzer powered by a 15 MW PV park by combining wind power and battery storage – feasibility study. Int J Hydrogen Energy 2018;43:16468–78. https://doi.org/10.1016/j.ijhydene.2018.07.069.
[33] Tang O, Rehme J, Cerin P. Levelized cost of hydrogen for refueling stations with solar PV and wind in Sweden: on-grid or off-grid? Energy 2022;241:122906. https://doi.org/10.1016/j.energy.2021.122906.
[34] Wei F, Dao M, Song P, Lu X, Zhang H, Zhang J, et al. Evaluation on the efficiency of a solar powered solid oxide

electrolysis cell plant for carbon dioxide reduction. Int J Electrochem Sci 2014;9:1146–62.
[35] Lo Franco F, Morandi A, Raboni P, Grandi G. Efficiency comparison of DC and AC coupling solutions for large-scale PV+BESS power plants. Energies 2021;14:4823. https://doi.org/10.3390/en14164823.
[36] Xavier LS, Amorim WCS, Cupertino AF, Mendes VF, do Boaventura WC, Pereira HA. Power converters for battery energy storage systems connected to medium voltage systems: a comprehensive review. BMC Energy 2019;1:7. https://doi.org/10.1186/s42500-019-0006-5.
[37] Ghenai C, Bettayeb M, Brdjanin B, Hamid AK. Hybrid solar PV/PEM fuel Cell/Diesel Generator power system for cruise ship: a case study in Stockholm, Sweden. Case Stud Therm Eng 2019;14:100497. https://doi.org/10.1016/j.csite.2019.100497.
[38] Tyagi VV, Rahim NAA, Rahim NA, Selvaraj JA/L. Progress in solar PV technology: research and achievement. Renew Sustain Energy Rev 2013;20:443–61. https://doi.org/10.1016/j.rser.2012.09.028.
[39] Kavlak G, McNerney J, Trancik JE. Evaluating the causes of cost reduction in photovoltaic modules. Energy Pol 2018;123:700–10. https://doi.org/10.1016/j.enpol.2018.08.015.
[40] Saba SM, Müller M, Robinius M, Stolten D. The investment costs of electrolysis – a comparison of cost studies from the past 30 years. Int J Hydrogen Energy 2018;43:1209–23. https://doi.org/10.1016/j.ijhydene.2017.11.115.
[41] Making the breakthrough: green hydrogen policies and technology costs n.d.:68.
[42] Green hydrogen cost reduction: scaling up electrolysers to meet the 1.5C climate goal n.d.:106.
[43] Kabouche N, Meziane F, Nouicer I, Boudries R. Comparative study of different PV systems configurations combined with alkaline and PEM water electrolyzers for hydrogen production. In: Khellaf A, editor. Advances in renewable Hydrogen and Other Sustainable Energy Carriers. Singapore: Springer; 2021. p. 481–9. https://doi.org/10.1007/978-981-15-6595-3_62.
[44] Carmo M, Fritz DL, Mergel J, Stolten D. A comprehensive review on PEM water electrolysis. Int J Hydrogen Energy 2013;38:4901–34. https://doi.org/10.1016/j.ijhydene.2013.01.151.
[45] Rashid M, Al Mesfer M, Naseem H, Danish M. Hydrogen production by water electrolysis: a review of alkaline water electrolysis, PEM water electrolysis and high temperature water electrolysis. Int J Eng Adv Technol 2015:2249–8958. ISSN.
[46] Gutiérrez-Martín F, Amodio L, Pagano M. Hydrogen production by water electrolysis and off-grid solar PV. Int J Hydrogen Energy 2021;46:29038–48. https://doi.org/10.1016/j.ijhydene.2020.09.098.
[47] Monforti Ferrario A, Cigolotti V, Ruz AM, Gallardo F, García J, Monteleone G. Role of hydrogen in low-carbon energy future. In: Technologies for Integrated Energy Systems and Networks. John Wiley & Sons, Ltd; 2022. p. 71–104. https://doi.org/10.1002/9783527833634.ch4.
[48] Explorador Solar Chile n.d. https://solar.minenergia.cl/inicio (accessed January 31, 2022).
[49] Sengupta M, Xie Y, Lopez A, Habte A, Maclaurin G, Shelby J. The national solar radiation data base (NSRDB). Renew Sustain Energy Rev 2018;89:51–60. https://doi.org/10.1016/j.rser.2018.03.003.
[50] Akar S, Beiter P, Cole W, Feldman D, Kurup P, Lantz E, et al. Annual technology baseline (ATB) cost and performance data for electricity generation technologies 2020. 2020. https://doi.org/10.7799/1644189.
[51] Package PySAM. National Renewable Energy Laboratory; 2022.
[52] Danecek P, Bonfield JK, Liddle J, Marshall J, Ohan V, Pollard MO, et al. Twelve years of SAMtools and BCFtools. GigaScience 2021;10:giab008. https://doi.org/10.1093/gigascience/giab008.
[53] Gilman P. SAM photovoltaic model technical reference. 2015. https://doi.org/10.2172/1215213.
[54] Stein J, Klise G. Models used to assess the performance of photovoltaic systems. Sandia National Laboratories; 2009. https://doi.org/10.2172/974415.
[55] Mayyas AT, Ruth MF, Pivovar BS, Bender G, Wipke KB. Manufacturing cost analysis for proton Exchange Membrane water electrolyzers. Golden, CO (United States): National Renewable Energy Lab. (NREL); 2019. https://doi.org/10.2172/1557965.
[56] Falcão DS, Pinto AMFR. A review on PEM electrolyzer modelling: guidelines for beginners. J Clean Prod 2020;261:121184. https://doi.org/10.1016/j.jclepro.2020.121184.
[57] Sorace R. Development and analysis of proton Exchange water electrolyzer (PEMWE) model with chemical degradation phenomenon. Master thesis. NTNU; 2021.
[58] Villagra A, Millet P. An analysis of PEM water electrolysis cells operating at elevated current densities. Int J Hydrogen Energy 2019;44:9708–17. https://doi.org/10.1016/j.ijhydene.2018.11.179.
[59] Hernández-Gómez Á, Ramirez V, Guilbert D. Investigation of PEM electrolyzer modeling: electrical domain, efficiency, and specific energy consumption. Int J Hydrogen Energy 2020;45:14625–39. https://doi.org/10.1016/j.ijhydene.2020.03.195.
[60] Yodwong B, Guilbert D, Phattanasak M, Kaewmanee W, Hinaje M, Vitale G. Faraday's efficiency modeling of a proton exchange membrane electrolyzer based on experimental data. Energies 2020;13:4792. https://doi.org/10.3390/en13184792.
[61] Sorace R. Development and analysis of proton Exchange Membrane water electrolyzer (PEMWE) model with chemical degradation phenomenon. MSc Thesis. NTNU Norwegian University of Science and Technology; 2021.
[62] Görgün H. Dynamic modelling of a proton exchange membrane (PEM) electrolyzer. Int J Hydrogen Energy 2006;31:29–38. https://doi.org/10.1016/j.ijhydene.2005.04.001.
[63] Selamet ÖF, Becerikli F, Mat MD, Kaplan Y. Development and testing of a highly efficient proton exchange membrane (PEM) electrolyzer stack. Int J Hydrogen Energy 2011;36:11480–7. https://doi.org/10.1016/j.ijhydene.2011.01.129.
[64] Ni M, Leung MKH, Leung DYC. Energy and exergy analysis of hydrogen production by a proton exchange membrane (PEM) electrolyzer plant. Energy Convers Manag 2008;49:2748–56. https://doi.org/10.1016/j.enconman.2008.03.018.
[65] Moradi Nafchi F, Baniasadi E, Afshari E, Javani N. Performance assessment of a solar hydrogen and electricity production plant using high temperature PEM electrolyzer and energy storage. Int J Hydrogen Energy 2018;43:5820–31. https://doi.org/10.1016/j.ijhydene.2017.09.058.
[66] Escobar-Yonoff R, Maestre-Cambronel D, Charry S, Rincón-Montenegro A, Portnoy I. Performance assessment and economic perspectives of integrated PEM fuel cell and PEM electrolyzer for electric power generation. Heliyon 2021;7:e06506. https://doi.org/10.1016/j.heliyon.2021.e06506.
[67] Tjarks G, Gibelhaus A, Lanzerath F, Müller M, Bardow A, Stolten D. Energetically-optimal PEM electrolyzer pressure in power-to-gas plants. Appl Energy 2018;218:192–8. https://doi.org/10.1016/j.apenergy.2018.02.155.
[68] Mayyas AT, Ruth MF, Pivovar BS, Bender G, Wipke KB. Manufacturing cost analysis for proton Exchange Membrane water electrolyzers. 2019. https://doi.org/10.2172/1557965.

[69] Caparrós Mancera JJ, Segura Manzano F, Andújar JM, Vivas FJ, Calderón AJ. An optimized balance of plant for a medium-size PEM electrolyzer: design, control and physical implementation. Electronics 2020;9:871. https://doi.org/10.3390/electronics9050871.

[70] Bessarabov D, Millet P. Chapter 1 - the PEM water electrolysis plant. In: Bessarabov D, Millet P, editors. PEM Water Electrolysis. Academic Press; 2018. p. 1–31. https://doi.org/10.1016/B978-0-08-102830-8.00001-1.

[71] Buttler A, Spliethoff H. Current status of water electrolysis for energy storage, grid balancing and sector coupling via power-to-gas and power-to-liquids: a review. Renew Sustain Energy Rev 2018;82:2440–54. https://doi.org/10.1016/j.rser.2017.09.003.

[72] Electrolyser PEM. Nel hydrogen. 2018. https://nelhydrogen.com/product/m-series-3/. accessed March 18, 2022.

[73] Lettenmeier P. Efficiency electrolysis - a siemens white paper. Siemens AG; 2019.